DATA: Diafiltration Apparatus for high-Throughput Analysis

Jonathan A. Ouimet, Xinhong Liu, David J. Brown, Elvis A. Eugene, Tylar Popps, Zachary W. Muetzel, Alexander W. Dowling, William A. Phillip*

> Department of Chemical and Biomolecular Engineering University of Notre Dame, Notre Dame, IN 46556

Abstract

Improved characterization techniques, which address knowledge gaps related to the interfacial

processes that govern solute-solute selectivity and the performance of membranes in complex multi-

component feed streams, are necessary to advance membrane processes. In this study, guided by

the tools of data science, a diafiltration apparatus is developed to inform material and process

design by rapidly characterizing membrane performance over a broad range of feed solution compo-

sitions. The apparatus doses a fixed-concentration diafiltrate solution into a stirred cell to achieve

a predetermined change in the retentate concentration. Here, using an 80 mM potassium chlo-

ride (KCl) diafiltrate solution, it was shown that membrane performance, within a 5 mM to 80

mM KCl phase space, could be probed five times more quickly with one diafiltration experiment

(8 hours) than with an experimental campaign using traditional filtration processes (47 hours).

Additionally, the synergy between data analytics and instrumentation led to the incorporation of

an inline conductivity probe that monitored the real-time retentate concentration. This additional

information provided key insights to distinguish between the mechanisms that govern membrane

separations (e.g., discriminating between adsorption or rejection based separations) and allowed

for the membrane transport coefficients to be determined accurately. Ultimately, incorporating the

appropriate governing phenomena identified a single set of self consistent parameters for commercial

NF90 membranes.

Highlights:

• Synergy between data analytics and instrumentation enables innovative device design.

*Corresponding author

Email address: wphillip@nd.edu (William A. Phillip)

- DATA allows for the evaluation of membrane performance over a wide concentration range.
- Diafiltration experiments run five times faster than traditional experiments.
- An inline conductivity probe directly measures the retentate concentration.
- Modeling the appropriate physics identifies a single set of self-consistent parameters.

Keywords: diafiltration, nanofiltration, parameter estimation, high throughput experimentation, model calibration

Experimental Model Based Design **Data Analytics Sensitivity Analysis Model Predictions** Retentate Concentration Permeate

DATA: Diafiltration Apparatus for high-Throughput Analysis

Graphical Abstract

Time

σ

1. Introduction

Membrane processes have advanced separations that are critical to modern society (e.g., supplementing freshwater resources through seawater desalination [1], isolating and purifying therapeutic medicines [2, 3], and enriching nitrogen from air [4, 5]). These demonstrated successes, in conjunction with the continued demand for energy-efficient and sustainable unit operations, drives the development of higher performance membranes. A promising area for growth resides in the ability to tailor the solute-solute selectivity of membranes such that they are capable of separating molecules of similar sizes and chemistries [6, 7, 8]. The development of membranes with solute-tailored selectivity will require studying model systems to understand the fundamental thermodynamic and transport phenomena that govern their separation mechanisms as well as examining the capabilities of these mechanisms in the complex multicomponent feed streams that will be encountered in practice [9].

Recent materials advances toward the development of membranes with solute-tailored selectivities have been directed at precisely controlling nanostructure (e.g., using self-assembled block copolymers [10, 11], lyotropic liquid crystals [12, 13], metal organic frameworks (MOFs) [14], and covalent-organic frameworks (COFs) [15, 16]) and manipulating chemistry to facilitate separations based on molecular identity rather than steric hindrance. For instance, COF membranes have exemplified the molecular control that can be exerted over the porosity and crystallinity of materials by carefully selecting polymeric precursors [16]. On the other hand, charge patterned mosaic membranes have been shown to preferentially permeate symmetric monovalent salts due to electrostatic interactions between the membrane and dissolved ions [17]. Similarly, Sadeghi et al. demonstrated that ligand binding effects can be used to tune the selective transport of similarly sized species through nanopores [18]. More recently, several efforts have focused on mimicking the highly selective and highly permeable nature of biological channels [19, 20, 21, 22]. In one instance, the growth of a zirconium based metal organic framework (MOF) within a polyethylene terephthalate membrane nanochannel modulated monovalent and divalent ion mobilities and consequently imparted the membrane with high monovalent: divalent ion selectivities [20].

The phenomena underlying the mechanisms of chemically-selective membranes are often based on multibody interactions and exhibit concentration dependencies [23, 24, 25]. As such, probing these dependencies can help to elucidate the molecular interactions and mechanisms that affect macroscopic transport properties. In turn, this knowledge can inform the design of higher performance membranes. As one example, there exists a trade-off between the magnitude of the solute-membrane affinity and the efficacy of the desired separation mechanism [24, 8]. When attractive forces are large, the membrane functions like an adsorbent binding the target solute molecules tightly, which provides minimal flux enhancements. Weak interactions lead to transport properties that are similar to those of size-selective filtration membranes. At an optimal, intermediate affinity, the flux of the target solute can be enhanced dramatically. On the other end of the spectrum, strong repulsive interactions increase the activation energy at the entrance of the pore and lead to solute rejection [26, 27]. Distinguishing between this array of potential transport mechanisms requires new methods that are better able to quantify membrane performance as a function of changing feed conditions. Developing these techniques will challenge preconceived hypotheses and dismiss

skewed results such as the notion that the high separation efficiency of some COF membranes were governed by rejection rather than adsorptive processes [15].

Improved characterization techniques would also benefit instances where the interaction between solutes in complex feed streams impact transport mechanisms. In one example, it has been shown that the negative rejection of potassium chloride within mixed salt systems increases as a function of the ionic strength [28]. Additionally, in separations where the pores and solutes are similar in size, the solutes may compete for entry into the pore [29]. This can lead to a decrease in the permeation of one species in the presence of a competing solute which possesses a higher affinity towards the membrane [18]. Intermolecular binding between solutes can also effect the efficiency of separations. For example, strong attractive interactions between albumin and a contaminating D-tryptophan impurity lead to a significant increase in the volume of diafiltrate required to obtain a product with the desired purity [30]. These examples illustrate how the advances in characterization of membranes deployed in complex multi-component feed streams, where solute-solute and solute-membrane interactions convolute the performance otherwise observed within single solute experiments, can benefit material and process development. For instance, Ghosh et al. [31, 32] demonstrated that pulsed sample injection techniques can systematically scan experimental parameters to identify optimal operating conditions for solute fractionation. This advanced scanning technique was used to create a complete profile of the observed sieving coefficient as a function of pH. The trends observed highlighted the dependence of protein conformation and protein dimerisation on transport phenomena. In turn, this insight reduced the time and resources necessary to determine process parameters.

The tools of data science can guide the design and optimization of the membrane-based separation processes [33]. For example, nonlinear parameter estimation is becoming increasingly important to validate mathematical models and characterize membrane performance in complex environments (e.g., mixed electrolyte solutions) [34, 35, 36]. Additionally, the emergence of techniques including model based design of experiments (MBDoE) enables the design of instruments to better characterize the performance of separation devices as a function of solute concentration and in complex feed streams. As such, these techniques can calculate the optimal conditions under which experiments must be run [37]. These results can be used to discriminate between alternative models [38, 39, 40] and provide key insight into how molecular level changes impact macroscopic system performance. In recent applications, MBDoE was used to propose a sequence of experiments that minimized the

experimental time and the resources required while improving the precision of parameter estimates for electrodialysis model identification [41]. Similarly, it has been shown that MBDoE can design one set of experiments to simultaneously improve parameter estimation as well as discriminate between competing kinetic models [42]. In order to use these tools to their full potential, we require models, based on first principles, and the ability to produce large amounts of data in an energy and time efficient way.

Traditional experimental campaigns with dead end filtration cells and cross flow devices are time consuming when used to elucidate membrane performance as a function of concentration. Furthermore, they typically infer the retentate concentration from the permeate concentration, implicitly assuming that solutes do not adsorb onto the membrane. Additionally, by running at near zero percent recoveries, they fail to capture the finite recoveries that commercial processes operate under. As a result, many experiments are necessary in order to capture membrane performance as the feed concentration changes over the course of an experiment. To exacerbate these limitations, traditional analyses, ones in which the local slope is linearly regressed from limited data sets, are unable to capture nonlinear trends well. These dynamic systems and corresponding time-series data must be modeled and analyzed with more advanced methods (e.g., differential algebraic equations, nonlinear parameter estimation, dynamic optimization) [43, 44].

In this study, guided by the tools of data science, limitations of current membrane characterization methods are addressed through the design of a diafiltration apparatus. A dead end stirred cell is modified to receive a high concentration diafiltrate such that high-throughput membrane characterization can be conducted over a broad range of concentrations. To begin, the rate at which an expanded range of concentrations can be explored by diafiltration when compared to traditional filtration techniques is examined. Then, data analytics are utilized to identify the experiments that are necessary to accurately regress characteristic membrane parameters in a lumped parameter model. This analysis is followed by a discussion on how data analytics can provide insight to guide the design of the experimental apparatus. Specifically, the addition of an inline conductivity probe that can monitor the real time trajectory of the solute concentration from the initial feed solution to the final retentate solution is detailed. The discussion finishes by evaluating how the proposed statistical frameworks can be used to distinguish between competing models and suggests that the diafiltration device can serve as a foundation to probe the concentration dependencies of chemically selective membranes, closing the knowledge gaps that exists between filtration experiments.

2. Mathematical Model

105

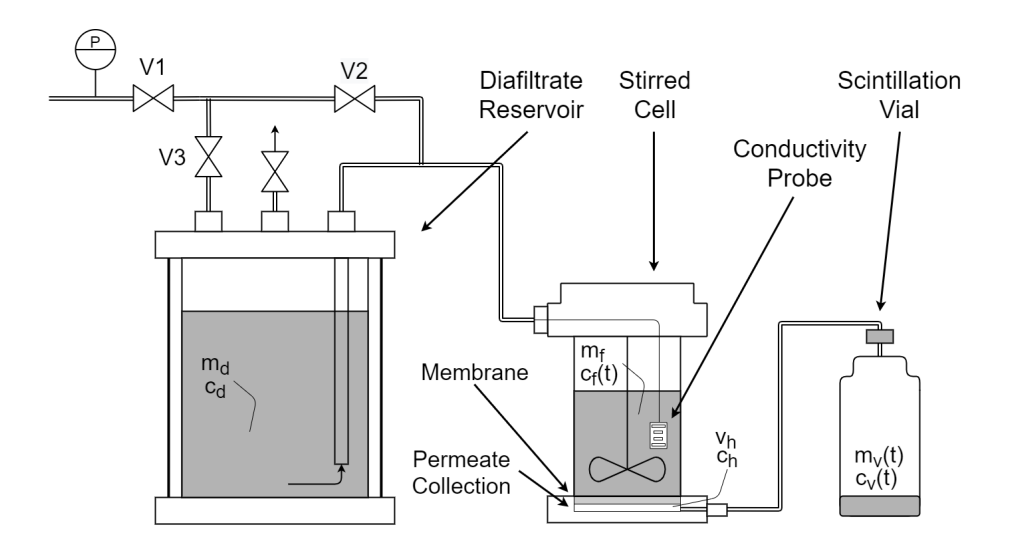


Fig. 1: A schematic of the experimental apparatus. The diafiltrate reservoir and stirred cell are loaded with solutions of known initial concentrations (i.e., $c_f(0)$ for the feed and c_d in the diafiltrate). After the apparatus is initialized, an applied pressure, P, feeds the diafiltrate into the stirred cell at a flow rate equal to the flow rate of permeate into the scintillation vial. The apparatus continuously monitors permeate mass (m_v) by using a scintillation vial resting on top of a balance. The concentrations of dissolved ions in the permeate are determined through inductively coupled plasma optical emission spectroscopy while the retentate concentration is monitored through an inline conductivity probe. The pressure is recorded using a digital pressure transducer attached to a gas reservoir.

The diafiltration apparatus presented in Fig. 1 allows for membrane characterization under changing retentate concentrations. In this study, a steady ramp in the retentate concentration is examined but a steady decrease in concentration is equally feasible. At the start of the experiment, the concentration in the stirred cell is low, ≈ 5 mM, and increases as the diafiltrate tank doses a high concentration salt solution into the cell at a rate equal to the volumetric flow rate of the permeate leaving. The volume under the membrane, where the permeate is collected, is termed the hold up volume and is modeled as a perfectly mixed reservoir. The tube connecting the stirred cell to the scintillation vial is assumed to act as a plug flow element where the salt solution is well mixed in the radial direction. An inline conductivity probe measures the retentate concentration within the stirred cell and a balance records the time dependent weight of the scintillation vial. The permeate within the scintillation vials are assumed to be well mixed and their concentration can be measured after the experiment.

A lumped parameter approach [45] is used to develop a physics-based mathematical model that captures the transport of solute and solvent within the experimental apparatus and through the membrane. The lumped parameter model used here assumes that diffusion is the dominant transport mechanism resulting in the solute flux being proportional to its concentration difference across the membrane. Additionally, it further assumes the feed side concentration is well mixed and changes more slowly than the rate the membrane responds (i.e., a pseudo steady state approximation is made when describing the solute flux). In previous works, this lumped parameter approach was combined with steady-state or time difference algebraic models for membrane parameter estimation [46, 47]. In contrast, this work develops a dynamic (e.g., differential algebraic equation) modeling framework that fully exploits the information contained in the collected time-series data.

The volumetric flux of water, J_w , and the molar flux of the solute, J_s , across the membrane can be expressed by Eqs. (1) and (2), respectively.

$$J_w = L_p(\Delta P - \sigma \Delta \pi)$$

$$= L_p[\Delta P - \sigma nRT(c_{in} - c_h)]$$
(1)

$$J_s = B(c_{in} - c_h) (2)$$

Here, we seek to estimate three model parameters, the hydraulic permeability, L_p , the solute permeability coefficient, B, and the thermodynamic reflection coefficient, σ , from experimental data. Mathematically, Eq. (1) makes it clear that to deconvolute L_p and σ , experiments at different applied pressures, ΔP , or experiments with different concentrations across the membrane, $c_{in} - c_h$, are necessary. Diafiltration easily satisfies the latter requirement. Within the above equations, $\Delta \pi = nRT(c_{in} - c_h)$ is the osmotic pressure, which, assuming the van't Hoff equation, is expressed in terms of n the number of dissolved species formed by the solute(s), R the gas constant, T the temperature, c_{in} the feed-side concentration at the solution-membrane interface, and c_h the concentration in the holdup volume, v_h . The difference in concentration across the membrane is represented by $c_{in} - c_h$, where c_{in} is related to the bulk feed concentration, c_f , by a thin film model that accounts for concentration polarization, Eqs. (3) and (4) [48].

$$\frac{c_{in} - c_h}{c_f - c_h} = \exp\left(\frac{J_w}{k}\right) \quad \Leftrightarrow \quad c_{in} = (c_f - c_h) \exp\left(\frac{J_w}{k}\right) + c_h \tag{3}$$

$$\frac{kb}{D} = 0.23 \left(\frac{bv^0}{\nu}\right)^{0.57} \left(\frac{\nu}{D}\right)^{0.33} \quad \Leftrightarrow \quad k = 0.23 \frac{(v^0)^{0.57} D^{0.67}}{\nu^{0.24} b^{0.43}} \tag{4}$$

where k is the mass transfer coefficient, b is the stirred cell diameter, D is the diffusion coefficient of the solute in water, ν is the kinematic viscosity of water, and v^0 is the average velocity within the system (i.e., the product between the stir bar angular velocity and radius).

In order to infer the three governing parameters in equation (1) and (2), we conduct mass and solute balances around three control volumes within Fig. 1, the diafiltrate reservoir, the stirred cell, and the permeate. Consequently, it is shown in the supporting information that the following ordinary differential equations (ODEs) describe the state of the system, equations (5)-(8).

$$\frac{dc_f}{dt} = \frac{A_m \rho}{m_f} (J_w c_d - J_s) \tag{5}$$

$$\frac{dc_h}{dt} = \frac{A_m \rho}{m_h} (J_s - c_h J_w) \tag{6}$$

$$\frac{dm_v}{dt} = -\frac{dm_d}{dt} = A_m \rho J_w \tag{7}$$

$$\frac{d(c_v m_v)}{dt} = \frac{dm_v}{dt} c_h = A_m \rho J_w c_h \tag{8}$$

where A_m is the membrane area, ρ is the density of the solution, m_f is the mass of the filtration cell, c_d is the diafiltrate concentration, m_h is the mass of solution in holdup, m_v is the mass of the sample vial, m_d is the mass of the diafiltrate reservoir and c_v is the concentration in the sample vial.

150

Adding concentration polarization, which is modeled with the algebraic Eq. (3), to the ODEs above, forms a system of differential algebraic equations (DAEs) to describe the dynamic process. Both the ODE and DAE models are numerically integrated in MATLAB using ode15s to simulate the diafiltration experiments. Specially, $c_v \cdot m_v$ is selected as a combined state variable for better initialization and to avoid division by zero. For the initial conditions of the first vial, c_f is set as the retentate concentration measurement at the beginning of the experiment, c_h is approximated at 80% of the first vial concentration, m_v is approximated as the mass of one drop of solution (≈ 0.05 g), and $c_v \cdot m_v$ is set as zero. To simulate vial swaps, the integrator is stopped and the initial

conditions are updated: c_f , c_h and $c_v \cdot m_v$ are set as the final condition of the previous vial and m_v is reset to the mass of one drop. Equation (8) is integrated instead of Eq. (S9) because c_v is not defined when $m_v \approx 0$ (empty vial).

3. Materials and Methods

3.1. Materials and Equipment

An Amicon 8010 stirred cell (Amicon, Burlington, Massachusetts) was used in all experiments. NF90 membranes supplied by DuPont (DuPont, Wilmington, Delaware) were used for all of the experiments. Pressure data was monitored using an Omega PX409 USBH pressure transducer (Omega, Norwalk, Connecticut). Mass data was measured by an OHAUS Adventure Series Balance (OHAUS, Parsippany, New Jersey). Conductivity data was gathered from an LFS 1107 conductivity sensor (Innovative Sensor Technology, Las Vegas, Nevada). A Keithly 6221 DC and AC current source function generator (Keithly, Cleveland, Ohio) was used to generate a 1 mA peak to peak sinusoidal AC current. The voltage drop across the conductivity sensor electrodes was measured with a GwInStek GDS 1054B oscilloscope (GwInStek, Montclair, California). The information was converted to a conductivity measurement and used in further analyses. An in-house MATLAB code was used to synchronize and record mass, conductivity and pressure data. All salt solutions were prepared using deionized water (DI water) that was supplied by a Millipore water purification system (Milli Q Advantage A10, Milli Q, MA). Potassium chloride (KCl), and nitric acid (HNO3) were purchased from Sigma Aldrich (Aldrich, St. Louis, Missouri) and had purities greater than 99.0% and 70% respectively.

3.2. Hydraulic Permeability Measurements

180

The hydraulic permeabilities of the NF90 membranes were determined by placing the flat sheet membrane into an Amicon stirred cell. The stirred cell volume above the membrane was filled with 10 mL of DI water. Nitrogen gas was used to apply pressures between 30 psi and 60 psi. The water permeated through the membrane was collected in scintillation vials that rested on top of the OHAUS balance. A computer logged the mass and pressure data over time. This data was used to calculate the hydraulic permeability of the membrane.

3.3. Filtration Experiments

Filtration experiments were carried out in a 10 mL Amicon stirred cell. The stirred cell was loaded with 12 mL of feed solution at predetermined salt concentration. The stirred cell was placed on a stir plate and stirred (at atmospheric pressure) for 10 minutes to allow ion adsorption onto the membrane and exposed surfaces of the stirred cell to take place. 1 mL of the feed solution was subsequently removed from the stirred cell and stored in a scintillation vial to be analyzed by Inductively Coupled Plasma Optical Emission Spectroscopy (ICP-OES). The conductivity probe was turned on and nitrogen gas was used to apply a pressure of 60 psi to the stirred cell. A pressure transducer, in series with the cell, was used to monitor the applied pressure and a balance recorded the mass of permeate in the scintillation vials. At each 0.5 mL of permeate, the scintillation vials were replaced, sealed and stored for further analysis. The mass, pressure, and conductivity readings of the three instruments were synchronized by a MATLAB code that recorded the time dependent data. At the end of the experiment, the retentate and the solution left within the tube between the stirred cell and the scintillation vial were collected. All closed sample vials were stored until they were prepared for analysis by ICP-OES. After each experiment, the conductivity probe was cleaned with DI water and subsequently stored in DI water until the next experiment was conducted.

3.4. Diafiltration Experiments

Diafiltration experiments were conducted within a modified stirred cell apparatus (Fig. 1). The diafiltrate tank was filled with a high concentration salt solution. A portion of this solution was collected and stored within a scintillation vial for further analysis by ICP-OES. A 10 mL Amicon stirred cell was prepared with 11 mL of a salt solution. The solution was stirred for 10 minutes to allow any ion adsorption onto the membrane to occur. 1 mL of the resulting feed solution was collected and stored.

The mathematical analysis of the data was conducted under the assumption that the flow rate of diafiltrate into the stirred cell was equal to the flow rate of permeate out of the stirred cell. To achieve this condition experimentally, the volume of air between the diafiltrate tank and the stirred cell needs to compress into the headspace of the stirred cell. We cannot start the experiment from atmospheric pressure because, once increased to the operating pressure, there are not enough gas molecules within the tubing to occupy the headspace of the stirred cell (i.e., the diafiltrate would flood the stirred cell in an uncontrolled manner). For the current experimental system,

the volume of air between the tank and stirred cell is 35 mL and the headspace volume is 7 mL. Assuming an ideal gas, the pressure of the system immediately before starting the experiment, must be 1/6 of the operating pressure to minimize overflow of diafiltrate into the stirred cell. To pressurize the system, valve 1 (V1) was opened, valve 2 (V2) was opened, and valve 3 (V3) was closed. The tank and stirred cell were pressurized to 1/6 of the operating pressure. Valve 1 was left open, valve 2 was closed and valve 3 was opened. The system was then subject to the operating pressure of 60 psi. This pressure pushed the diafiltrate solution up into the tubing and towards the stirred cell. The small bolus of diafiltrate that enters the stirred cell, termed the overflow, is measured to be the difference in mass between the initial feed solution (before start-up) and the retentate (end of experiment after shut-down). With known feed and diafiltrate concentrations, this information is used to calculate the concentration of the feed at the start of the experiment. The initial concentration is also corroborated by the measurement taken by the inline conductivity probe.

Immediately after increasing the pressure to the operating pressure, the mass, retentate conductivity and pressure are synchronized and recorded at five second intervals. Scintillation vials that rest on top of a balance are used to collect permeate samples at 1 mL intervals. A total of 10 scintillation vials are collected throughout the course of the experiment. After the collection of the last permeate vial, valve 1 is closed and the pressure relief valve is opened, releasing the pressure of the diafiltrate tank and causing the compressed air in the headspace of the stirred cell to expand, pushing the diafiltrate solution back into the diafiltrate reservoir. The retentate and the solution in the tubing between the stirred cell and the scintillation vial were collected in separate scintillation vials. The scintillation vials were closed and stored until they could be analyzed on ICP-OES. The conductivity probe was turned off, rinsed with DI water and stored in DI water until the next experiment was conducted.

3.5. ICP-OES Sample Preparation

The concentration of the salt within all collected samples was analyzed by ICP-OES (Perkin Elmer Optima 8000). All experimental samples were prepared with calibrated micropipettes. Filtration experiment samples were prepared by diluting 0.100 mL of sample with 5.00 mL of 3% nitric acid. The samples were labeled and stored in falcon tubes. The feed and permeate samples of diafiltration experiments were prepared analogously to filtration experiments samples. Due to their

higher concentrations, the diafiltrate and retentate samples from diafiltration experiments were prepared by diluting 0.025 mL of sample with 5.00 mL of 3% nitric acid. We note that all samples were interpolated within calibration curves in which the correlation coefficients were greater than 0.995.

3.6. Design and Retrofitting of Inline Conductivity Probe

The stirred cell was retrofit with an LFS 1107 Conductivity Sensor. The six leads were soldered and connected to 28-gauge space saver wire (McMaster Carr, Elmhurst, Illinois). The bare metal leads were potted with DP420 Scoth-Weld Epoxy Adhesive (3M, Saint Paul, Minnesota). The leads of the conductivity probe were threaded through the inlet of the Amicon stirred cell. The wires were then maneuvered through one end of a 1/4 inch Swagelok compression union tee (Swagelok, Solon, Ohio). The current wires were connected to the Keithly 6221 DC and AC current source which generated a 1 mA peak to peak sine wave. The voltage wires of the conductivity probe were connected to the GwInStek GDS 1054B oscilloscope. Time dependent voltage measurements were recorded throughout the course of the experiment. The conductivity of the retentate solution was determined from the current, voltage and cell constant data.

3.7. Calibration of Inline Conductivity Probe

The LFS 1107 conductivity sensor was calibrated with 7 KCl stock solutions spaced between 0 mM and 100 mM. The probe was submerged into the stock solution, given 5 seconds to stabilize and the amplitude of the voltage drop was recorded from the GwInStek GDS 1054B oscilloscope. The probe was rinsed with DI water after each measurement. The resulting data were linearly regressed to produce a calibration curve that has a correlation coefficients greater than 0.99 (Fig. S1). The calibration curve was used to relate the conductivity readings to the internal concentration of the stirred cell.

4. Results and Discussion

4.1. Experimental filtration data sets

A representative set of filtration data is presented in Fig. 2. The mass of the permeate is plotted versus time in Fig. 2A. Samples are collected in scintillation vials at 0.5 mL intervals. As such, the sudden drops in mass correspond to a switch of the collection vial. The solution within these

vials is then prepared for analysis by ICP-OES. As highlighted within Fig. 2B, the concentration of salt within the permeate samples changes slightly. Provided that the initial feed concentration is known and assuming no salt adsorbs to the membrane, a mass balance can be used to infer the internal concentration of the stirred cell. The measurements from the conductivity sensor, purple squares in Fig. 2B, corroborate the concentration of dissolved salt from these calculations (Fig. S2A). The agreement between the measured data points and calculations confirm that the mass balance on potassium chloride closes. Using the retentate and permeate concentrations from each vial a percent rejection of 70% is calculated from the experimental results, which is consistent with the value reported in the literature [49].

Although this approach is more useful than operating at zero percent recovery, filtration experiments are still limited because they rely on the rejection of solutes to drive changes in the retentate concentration. Even for solutes that are highly rejected, this approach leads to modest variations in the solute concentration. As solvent permeates through the membrane, the concentration of the rejected species within the feed begins to increase. Assuming 100% percent rejection, the concentration of the solute will double when the solvent volume is reduced by half (i.e., 50% recovery). Within Fig. 2A, the experiment is run at approximately 40% recovery and the retentate concentration changes 2-3 mM. Fig. S2B presents that data for an experiment, run at 60% recovery. A similar change in concentration is observed in this experimental data but it highlights an additional issue with filtration, the high recovery experiments are incompatible with the inline conductivity sensor, which must be submerged to be utilized. Consequently, many filtration experiments are necessary in order to characterize membrane properties over large concentration ranges.

4.2. One diafiltration experiment generates knowledge five times faster than filtration experiments

The diafiltration apparatus addresses the drawbacks of filtration experiments by dosing a concentrated diafiltrate solution into the stirred cell in a controlled manner, instead of relying on the rejection of solutes to drive an increase in the retentate concentration. During the operation of the apparatus, the volumetric flux of diafiltrate into the stirred cell is equal to the volumetric flux of permeate out. As such, the maximum retentate concentration that can be achieved may be estimated as the concentration of the diafiltrate divided by the sieving coefficient $(c_{r,max} = c_D \cdot S^{-1})$. Assuming that the osmotic pressure of the feed solution and concentration polarization are negligible, the sieving coefficient can be related to the model parameters through a series of substitutions,

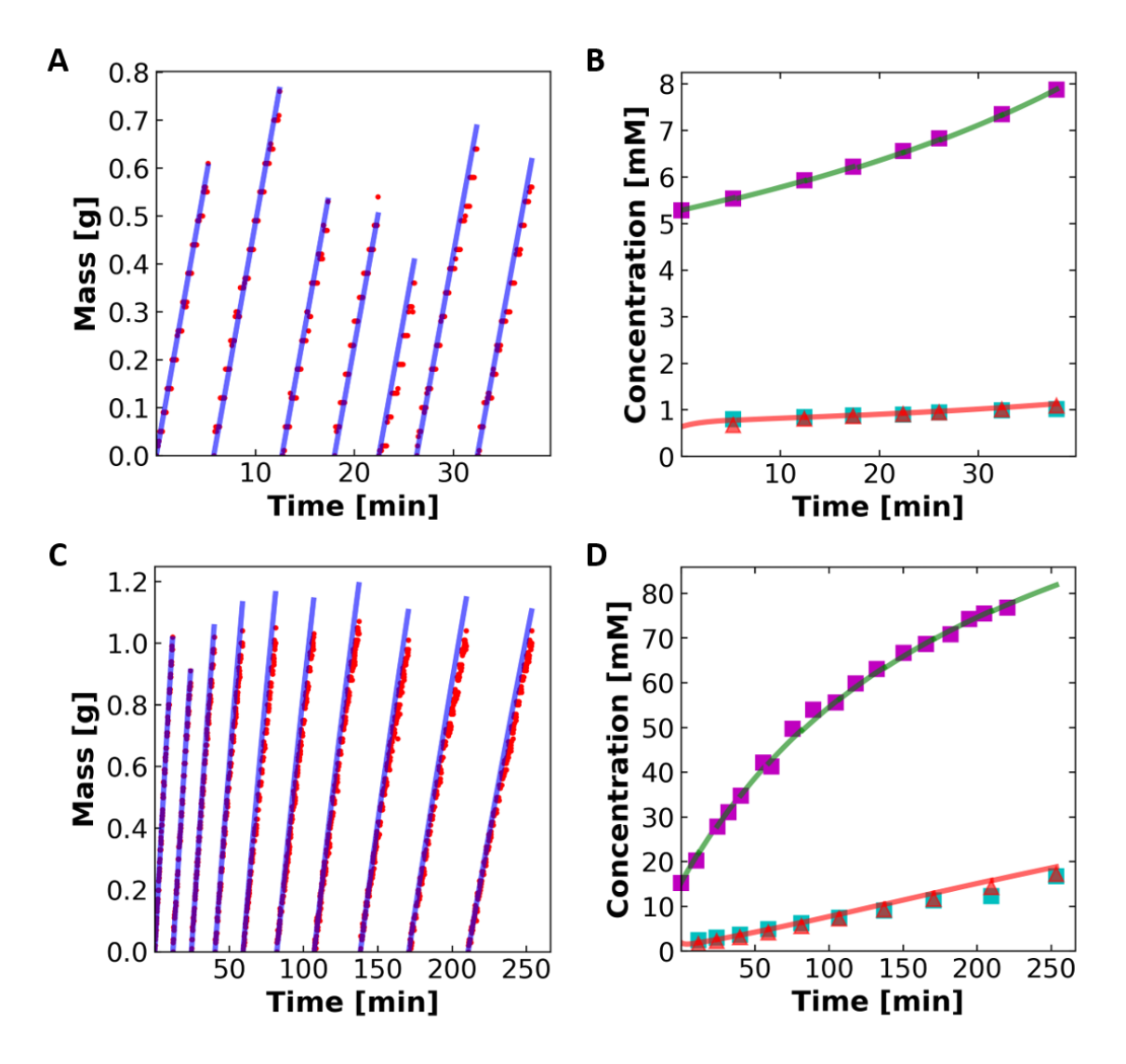


Fig. 2: Mass versus time data points from filtration (A) and diafiltration (C) experiments are compared to computational predictions, represented by the solid lines. Mass predictions are obtained from Eqs. (1) and (S9) utilizing the membrane A model A parameters from Tables 1 and 2. Experimental retentate concentrations, measured by a conductivity probe, and permeate vial concentrations, measured using inductively coupled plasma optical emission spectroscopy, for filtration (B) and diafiltration (D) experiments are plotted against computational predictions from equations (5) and (6), respectively. The red triangles within panels B and D, calculated using Eq. (S9), correspond to discrete predicted vial concentrations while the red line represents the continuous holdup concentration.

Eq. (9).

$$S = \frac{c_p}{c_f} = \frac{J_s}{J_w c_f} = \frac{B}{L_p \Delta P} (1 - S) \quad \Leftrightarrow \quad S = \frac{\frac{B}{L_p \Delta P}}{1 + \frac{B}{L_p \Delta P}} \tag{9}$$

In practice, the experiment may be limited by the solubility of the solute or the osmotic pressure of the feed solution. Nevertheless, the estimate is useful as it allows the experimental operations to be tailored such that the retentate concentration data are spaced evenly over a specified region of interest.

The purple squares within Fig. 2D correspond to the concentration of the retentate over the course of a diafiltration experiment. By starting at a low feed concentration (i.e., 10 mM) and dosing in a high concentration diafiltrate (i.e., 80 mM) the data points are spaced evenly over a 60 mM range. An effect of this wider range of retentate concentrations manifests in Fig. 2C, which presents the experimental permeate mass vs time data. In particular, the slope of the mass vs time data decreases throughout the experiment due to the increase in the osmotic pressure of the retentate. The sudden drops in the mass data correspond to a vial switch where permeate samples are collected for further analysis by ICP-OES. The permeate concentrations are presented in Fig. 2D as blue squares. Over the wider range of concentrations examined, the percent rejection for each vial is still consistent with the reported rejection of 70% [49].

A critical benefit of the diafiltration apparatus is captured graphically in Fig. 3. One diafiltration experiment can provide an equal or greater amount of information five times more quickly than several filtration experiments. Table S1 presents a full comparison of the time requirements for a representative set of filtration and diafiltration experiments. By combining high-throughput data collection and robust computational analytics, DATA is well suited to help address critical knowledge gaps related to the interfacial phenomena and multi-component interactions that govern membrane separation processes [9].

4.3. Computational modeling regresses governing membrane parameters

4.3.1. Computational predictions match experimental results

The experimental mass, permeate concentration, and retentate concentration data were used to characterize membrane performance in terms of a model based on lumped parameters, i.e., the hydraulic permeability, the reflection coefficient, and the solute permeability coefficient. These parameters are estimated using weighted nonlinear regression shown in Eq. (10). Here each set of

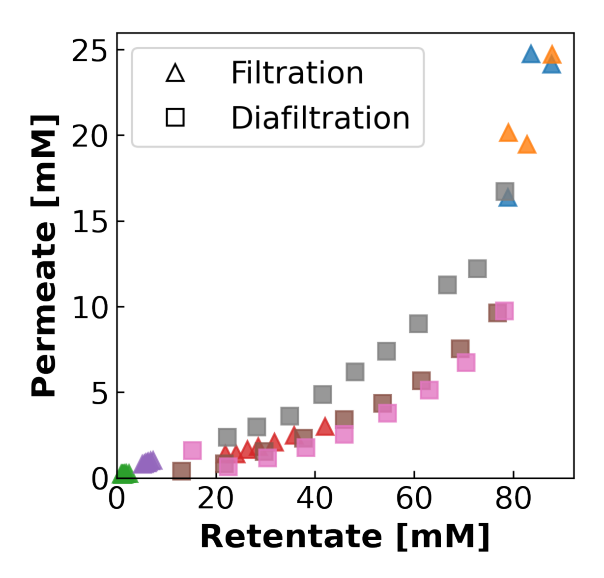


Fig. 3: The phase space of retentate concentrations and permeate concentrations explored by filtration and diafiltration experiments. Every color corresponds to a unique experiment. Filtration experiments are represented by triangular data points and diafiltration experiments are represented by square data points. Diafiltration experiments were conducted at an initial feed concentration of 15 mM KCl and a diafiltrate concentration of 80 mM KCl. The grey squares present diafiltration experiments for Membrane A. The brown and pink squares correspond to diafiltration experiments for Membrane D. Five filtration experiments were run at varying feed concentration ranging from 1 mM KCl to 75 mM KCl. The low concentration filtration experiments conducted at 1 mM (green triangles) and 5 mM (purple triangles) KCl each include 6 data points.

data (i.e., mass, permeate, retentate) were normalized by the measurement precision (i.e., $s_{m_v} = 0.01$ g, $s_{c_v,i} = 3.0\% \cdot c_{v,i}$, $s_{c_f,i} = 0.3\% \cdot c_{f,i}$) squared and the total number of measurements in the vial (i.e., $N_{m_v,i}$ is 70 to 500, $N_{c_v,i}$ is 1, $N_{c_f,i}$ is 0 (omitted) to 3, depending on the experiment). For example, the mass measurement $m_{v,i}$ was normalized by the weight $w_{m_v,i} = (s_{m_v}^2 N_{m_v,i})^{-1}$.

$$\hat{\theta} = \arg\min_{\theta} \sum_{i} w_{m_{v},i} (m_{v,i} - \hat{m}_{v,i})^{2} + \sum_{j} w_{c_{v},j} (c_{v,j} - \hat{c}_{v,j})^{2} + \sum_{k} w_{c_{f},k} (c_{f,k} - \hat{c}_{f,k})^{2}$$
(10)

The best fit parameters for filtration and diafiltration experiments are reported in Table 1 and 2, respectively. As discussed below, these values were identified from experimental designs that were

informed by an iterative feedback loop between data analytics and instrumentation capabilities.

The solid lines within Fig. 2 represent computational predictions from the fully calibrated model.

The strong agreement between model and experiment in conjunction with the self-consistent nature of the transport coefficients demonstrate the utility of integrating statistical analyses and DATA.

Table 1: Filtration experiments for three membranes (i.e., Membranes A, B, C) were conducted. The hydraulic permeability, solute permeability coefficient and the reflection coefficient for two different models (with concentration polarization & without concentration polarization) and two data set variations (data with an inline conductivity sensor & data encompassing only the initial and final retentate measurements) are presented. Predictions within rows labeled M1 include concentration polarization and the inline conductivity probe measurements. The regressed parameters from rows labeled M2 use a reduced data set which excludes the semi-continuous retentate data. The M3 predictions evaluate a model in which the inline conductivity measurements are used yet concentration polarization is knowingly withheld. The M4 predictions use the reduced data set and do not include concentration polarization. Comparisons of the squared residuals should only be drawn between experiments with same number of data points (i.e., M1 to M3, and M2 to M4).

	Membrane	Model	L_p	В	ь	Mass Objective	Permeate Objective	Retentate Objective
			$L\cdot m^{-2}\cdot h^{-1}\cdot bar^{-1}$	$\mu \mathrm{m}\cdot \mathrm{s}^{-1}$	dimensionless	g^2	${ m mM}^2$	mM^2
		M1	4.37	29.0	1	1.02E-03	2.96E-03	3.35E-04
	<	M2	4.30	0.67	0.83	1.01E-03	2.87 E-03	5.51E-05
	¥	M3	4.32	0.79	П	1.03E-03	2.97 E-03	3.55E-04
		M4	4.16	0.79	0.48	1.03E-03	2.74 E-03	5.43E-05
		M1	4.45	0.78	1	1.69E-03	$8.19 \hbox{E-}03$	5.16E-04
D:14.004:00	Ω	M2	4.33	0.78	0.62	1.78E-03	7.95 E-03	1.74E-04
riitratioii	Q	M3	4.40	0.91	1	1.70E-03	8.22E-03	5.21E-04
		M4	4.17	0.92	0.18	1.82E-03	7.63E-03	1.72E-04
		M1	3.18	0.31	0.19	7.51E-04	4.21E-03	1.61E-04
	ζ	M2	3.41	0.31	1.00	7.16E-04	4.31 E-03	1.76E-05
)	M3	3.13	0.35	0.00	7.59E-04	4.19 E-03	1.55E-04
		M4	3.38	0.35	1.00	7.21E-04	4.31 E-03	1.76E-05

Table 2: Diafiltration experiments for three membranes (i.e., Membranes A, B, C) were conducted. The hydraulic permeability, solute permeability coefficient and the reflection coefficient for two different models (with concentration polarization & without concentration polarization) and two data set variations (data with an inline conductivity sensor & data encompassing only the initial and final retentate measurements) are presented. Predictions within rows labeled M1 include concentration polarization phenomena and inline conductivity probe measurements. The regressed parameters from rows labeled M2 use a reduced data set which excludes the semi-continuous retentate data. The M3 predictions evaluate a model in which the inline conductivity measurements are used yet concentration polarization is not accounted for. The M4 predictions use the reduced data set and do not account for concentration polarization.

	Membrane	Model	L_p	В	ь	Mass Objective	Permeate Objective	Retentate Objective
			$L\cdot m^{-2}\cdot h^{-1}\cdot bar^{-1}$	$\mu \mathrm{m}\cdot \mathrm{s}^{-1}$	dimensionless	$^{\circ}$	$^{ m v}$ $^{ m mM}^2$	$^{\circ}$ $^{ m mM}^2$
		M1	3.90	0.29	1	3.39E-03	7.31E-01	9.74E-01
	<	M2	3.25	0.31	1	3.27E-03	4.38E-01	5.52E-03
	¥	M3	3.68	0.31	1	4.49E-03	7.85E-01	1.10E+00
		M4	3.04	0.33	1	4.62E-03	4.53E-01	5.36E-03
		M1	3.42	0.50	1	5.30E-03	$2.11E{+}01$	1.23E+01
Dio 614 204102	Ω	M2	2.76	0.73	1	6.72E-03	7.30E+00	8.20E-05
Diamitation	٩	M3	3.27	0.53	1	6.37E-03	$2.23E{+}01$	1.41E+01
		M4	2.64	0.79	1	7.93E-03	7.25E+00	4.22E-04
		M1	2.74	0.34	0.88	5.76E-03	2.15E-01	4.52E+00
	ζ	M2	2.97	0.34	1.00	2.48E-03	4.33E-01	5.94E-03
)	M3	2.71	0.37	0.91	5.71E-03	2.73 E-01	4.42E+00
		M4	2.81	0.37	1.00	3.50E-03	4.28E-01	6.42E-03

4.3.2. High concentration experiments elucidate the reflection coefficient

Filtration experiments enable the estimation of the solute permeability and hydraulic permeability coefficients yet are incapable of identifying the reflection coefficient. Although the model predictions in Figs. 2A, 2B match the experimental data well, this is driven entirely by the estimates of L_p and B. Table 1 shows that while the reflection coefficient estimate is widely dependent on the data set, the value of the reflection coefficient utilized does not affect the quality of the computational fit.

The sensitivity analyses in Fig. 4A further demonstrates that the model predictions for the mass, permeate concentration, and retentate concentration are invariant to large perturbations in the reflection coefficient. Computational predictions assuming reflection coefficient values of 0.1, 0.5 and 0.9 resulted in indistinguishable, overlapping curves. Specifically, Fig. 4A displays the final permeate concentration is 1.1 mM KCl for any reflection coefficient value between 0.1 and 0.9. Likewise, the final retentate concentration only varies by 0.1 mM KCl when the reflection coefficient is adjusted from 0.1 to 0.9. The log transformed residual squared contours of the hydraulic permeability against the reflection coefficient presented in Fig. S5 (i.e., L_p vs. σ) also confirm that the model is insensitive to the reflection coefficient. These contours were generated using a 2-D grid search in which predictions are generated for all combinations of the two parameters. For example, Fig. S5A searches over the Lp and σ parameters while keeping the solute permeability coefficient constant. Likewise, Fig. S5B searches over Lp and B while keeping σ constant. Subsequently, comparing the predictions and experimental data allows for the residual squared error (e.g., for mass: $\sum_{i} (m_{v,i} - \hat{m}_{v,i})^2$) to be calculated. The log transformed residual values are then plotted to visualize the sensitivity as a function of the parameter estimates. These grid searches are conducted for each type of data collected (i.e., mass, permeate concentration, and retentate concentration). The sections of the contour that display a minima correspond to the optimal parameter combination that best fits the experimental data. Consequently, the horizontal iso-residual contours in Fig. S5 indicate that, at the optimal hydraulic permeability, any value of the reflection coefficient will provide an equivalent model fit. This confirms that the filtration experiments are insensitive to the reflection coefficient. This insensitivity, which makes the reflection coefficient unidentifiable, is due to the low retentate concentrations within the filtration experiments which produce negligible osmotic pressures in Eq. (1). Although no information can be gathered on the reflection coefficient, filtration experiments are capable of identifying membrane specific solute permeability coefficients

and hydraulic permeability coefficients as highlighted by the L_p vs. B contours presented in Fig. S6. The mass residual squared contour predicts the data can be best fit with an L_p value of 4.37 L \cdot m⁻² \cdot h⁻¹ \cdot bar⁻¹ and a solute permeability coefficient value of 0.67 μ m \cdot s⁻¹. This information is reinforced by the permeate and retentate contours which also display minimum squared residual values at the aforementioned L_p and B values(Fig. S6).

Diafiltration experiments overcome this limitation related to the osmotic pressure by exploring a broader concentration range. A sensitivity analysis (Fig. 4B) shows that dynamic model predictions are sensitive to perturbations in the reflection coefficient. At low retentate concentrations, three unique reflection coefficient values provide similar model predictions. Yet, the predictions diverge from one another once retentate concentrations greater than 40 mM are reached. Ultimately, after a four hour experiment, if the reflection coefficient of the membrane was equal to 0.1, the retentate concentration would be 163.5 mM KCl. Conversely, if the membrane reflection coefficient is equal to 0.5 or 0.9, the retentate concentration will be 112.9 mM KCl and 86.5 mM KCl, respectively. These differences are best highlighted within the retentate data, yet they are also apparent within the mass and permeate predictions. The threshold, where the predictions at varied reflection coefficient values diverge, is determined by the value of the osmotic pressure relative to the applied pressure.

The threshold can be reached by modulating the retentate concentration and applied pressure. Within filtration experiments, the retentate concentration is controlled by the initial feed concentration. For diafiltration experiments, the retentate concentration is modulated by the diafiltrate concentration. The contour maps in Fig. S7 highlight the experimental conditions necessary for filtration and diafiltration experiments to differentiate among reflection coefficient values that exhibit a 0.1 difference from one another. Specifically, Fig. S7A examines filtration experiment data while Figs. S7B, S7C, and S7D examine data presented at the end of the 1^{st} , 5^{th} , and 10^{th} vial of a diafiltration experiment, respectively. The lower right portion of the graphs shaded in grey corresponds to systems in which the water flux is equal to or less than zero (i.e., the osmotic pressure is equal to or greater than the applied pressure). Measurements are not plausible in this region. The contour lines show the difference in model predictions normalized by the equipment's precision. Notably, experimental conditions that generate contour values greater than two generate data capable of distinguishing the reflection coefficient differences of 0.1 or greater. The sensitivity analysis in Fig. S7A highlights the importance of capturing the retentate concentration accurately as the mass and permeate concentration measurements provide a limited amount of information

when identifying the true value of the reflection coefficient in filtration experiments. This is not the case for diafiltration experiments. After collecting the 5^{th} permeate vial, any experiment with a feed concentration of 5 mM KCl conducted with a diafiltrate concentration greater than 20 mM KCl and operating at an applied pressure greater than 30 psi is capable of identifying reflection coefficients that are 0.1 different. Consequently, diafiltration experiments allow the reflection coefficient to be captured more rapidly and under a wider number of operating conditions when compared to filtration experiments.

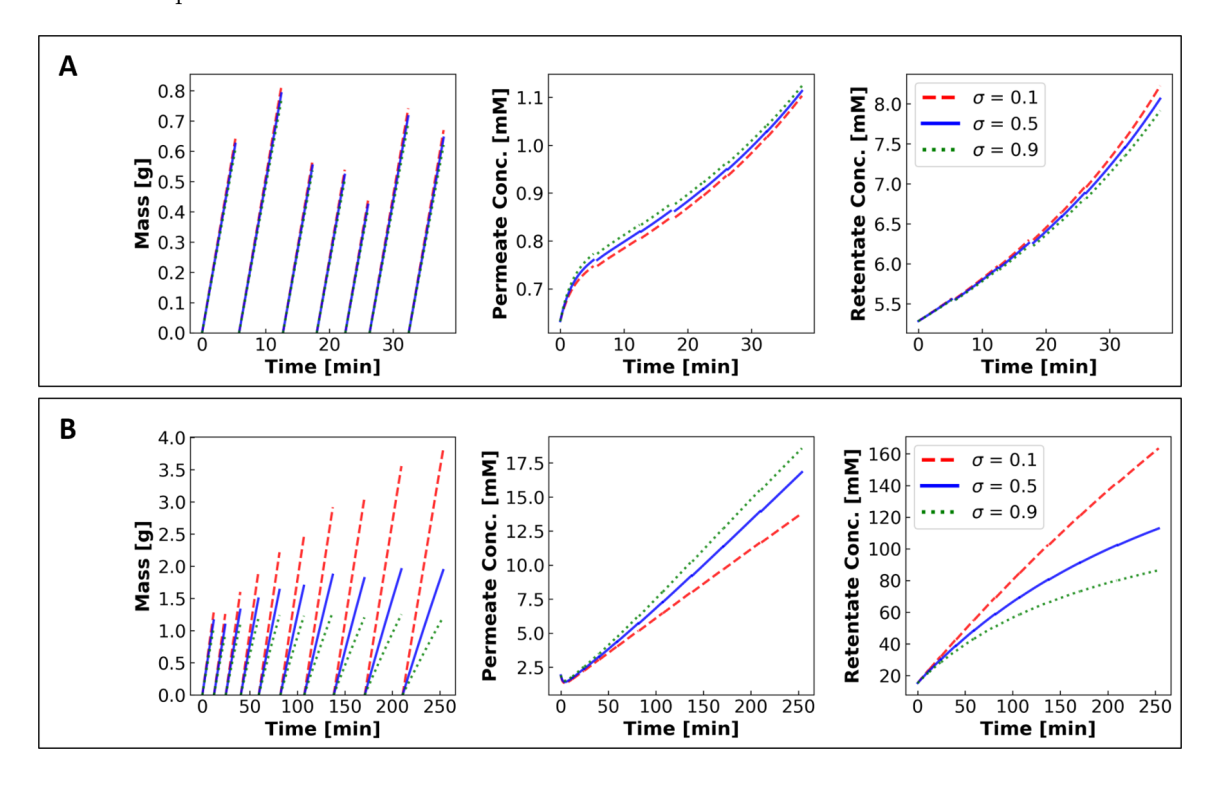


Fig. 4: Computational predictions display how different values of the reflection coefficient (i.e., $\sigma = 0.1, 0.5, 0.9$) affect the time evoluation of mass, retentate and permeate data. Physically, the reflection coefficient can take any value between zero and one. The predictions for were generated using equations (7) (left), (6) (middle) and (5) (right) with Lp & B values Membrane A, model M1 from Tables 1 and 2. At low concentrations, filtration predictions (A) cannot distinguish between different values of the reflection coefficients. While diafiltration predictions (B) for different reflection coefficients are indistinguishable at low concentrations, they diverge from one another at high concentrations.

4.3.3. Model parameters converge with the inclusion of an inline conductivity probe

Data analytics suggested the addition of an inline conductivity probe to the diafiltration apparatus to measure the concentration of the solution within the stirred cell. The measurements elucidate the path taken from the initial feed concentration to the final retentate concentration, therefore, providing two key benefits. First, as shown above and in Fig. 5A and 5B, it aids substantially in identifying a unique value of the reflection coefficient. Specifically, Fig. 5B presents regression contours in which only the initial feed and final retentate concentrations are used (i.e., no data from the inline conductivity probe). The local minima within the residual squared contours for the retentate concentration suggests that multiple combinations of the reflection coefficient and hydraulic permeability can fit the data set. This discrepancy is eliminated in Fig. 5A with the inclusion of the additional retentate concentration measurements. The three contours of Fig. 5A now converge to a unique value for the reflection coefficient (i.e., 1 [dimensionless]). When all data types converge to the same set of parameters, this suggests an accurate model. These findings show an inline conductivity sensor is needed in order to remove the local solutions and accurately elucidate the reflection coefficient of the membrane. Similar converging trends can be observed for the solute permeability coefficient and hydraulic permeability coefficient (Fig. 6). Fig. 5A and Fig. 6 suggest that the optimal value for the hydraulic permeability is $3.89 \text{ L} \cdot \text{m}^{-2} \cdot \text{h}^{-1} \cdot \text{bar}^{-1}$. At this L_p value, all three contours of Fig. 6A, provide an optimal solute permeability coefficient of $0.20 \ \mu \text{m} \cdot \text{s}^{-1}$.

Continuous monitoring of the retentate concentration is also beneficial because it provides evidence that the solute is rejected by the membrane and not removed by adsorptive processes. Distinguishing between rejection and adsorption provides critical knowledge for the development and application of new materials and membranes. Rejection-based and adsorption-based separation mechanisms can both result in low permeate concentrations. For membranes that reject dissolved species, the solute is retained in the solution above the membrane leading the retentate concentration to increase throughout the course of the experiment. In contrast, materials that act as sorbents reduce the retentate concentration while maintaining low permeate concentrations. As such, it is the distinct behavior of the retentate concentration that allows the underlying mechanism to be identified. In the experiments reported here, the retentate concentration measured using the inline probe increases. Moreover, the retentate concentration calculated from the permeate concentration measurements and a mass balance, shown as the green circles in Fig. S2B, agree well with the

inline measurements. This observation affirms that the NF90 membranes remove KCl through a rejection-based mechanism. While, based on prior knowledge, this outcome was expected for the NF90 membranes such distinctions are not as readily obvious for emerging materials that target solute-tailored selectivity [15, 8].

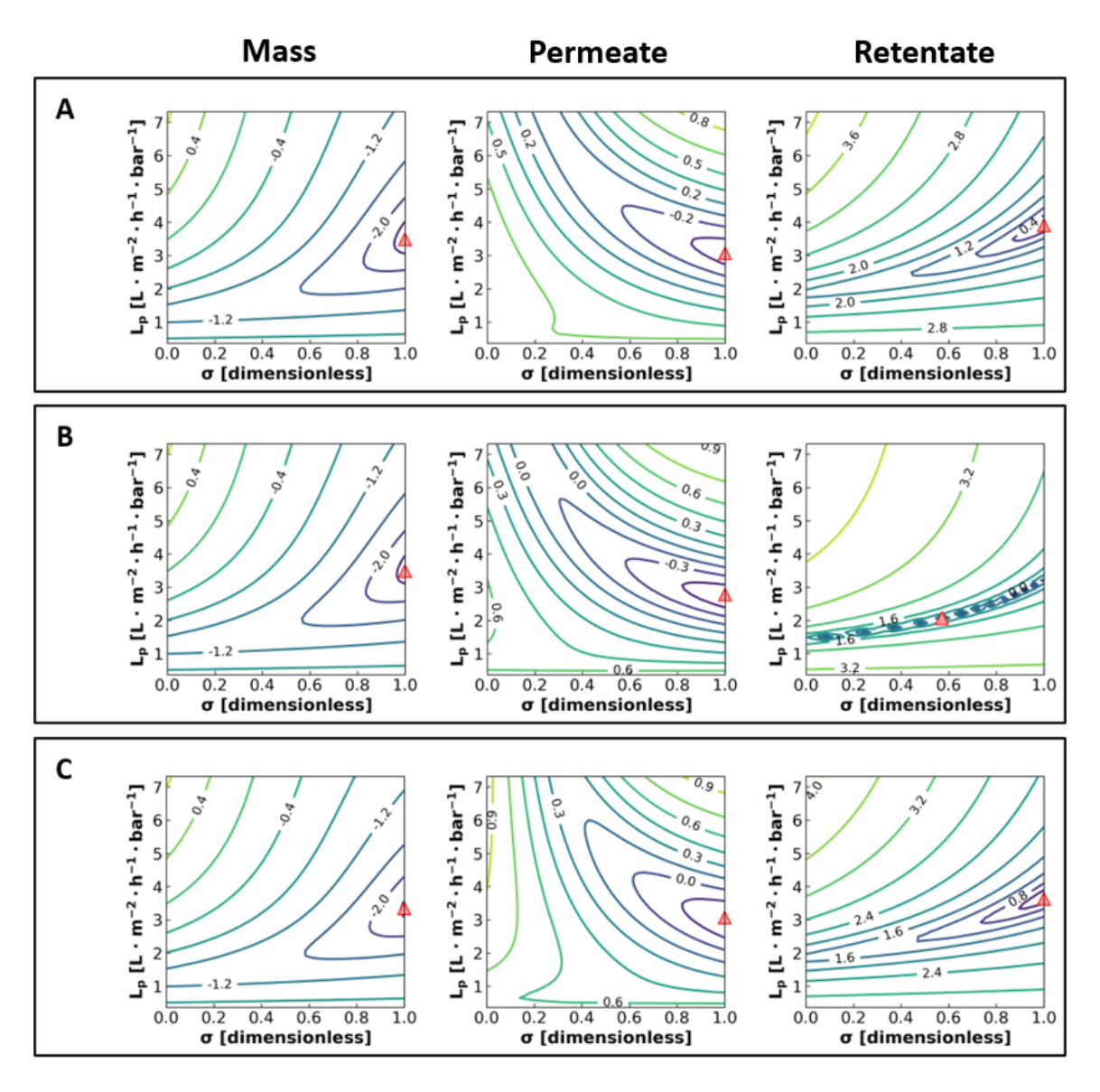


Fig. 5: Residual squared contours comparing the reflection coefficient and hydraulic permeability for **diafiltration** experiments. Two different models (with concentration polarization & without concentration polarization) and two data set variations (data with an inline conductivity sensor & data encompassing only the initial and final in-situ retentate measurements) are evaluated. The model used to generate the contours of panel A includes concentration polarization phenomena with the inline conductivity probe measurements. The residual squared contours of panel B were generated using a reduced data set which excludes the semi-continuous retentate data. Panel C contours evaluate a separate model in which the inline conductivity measurements are used yet concentration polarization is not accounted for.

4.3.4. Incorporating concentration polarization improves model predictions

Dynamic diafiltration experiments in tandem with data analytics facilitate the direct comparison of various model complexities and physical assumptions. For example, Fig. 5A and 5C explores how the residual squared contours change when concentration polarization effects are knowingly withheld from the modeling framework. As anticipated, the inclusion of concentration polarization provides improved estimates for all three model parameters. Moving from Fig. 5C to 5A, one notices the value of permeate contour lines decreases, this implies the mathematical model more accurately fits experimental results. In turn, permeate concentration contours increase the value of the optimal hydraulic permeability prediction. As a result, the L_p predicted from the mass, permeate, and retentate contours converge on a unique value and the residual squared objectives (displayed in Table 2) decrease. Additionally, within Fig. 5C, if σ is less than 0.4, the contour lines of Fig. 5C stretch vertically (This is exemplified by following the 0.6 contour line). This subtle change in the contours indicate that, by including concentration polarization, the model predictions become sensitive to the reflection coefficient.

Deployed more broadly, statistical learning frameworks including model-based design of experiments [50, 51, 52, 53] can guide the development of structure-function relationships that are critical to chemically selective transport mechanisms [33]. Given a model hierarchy [54], described by physics-based models, statistical learning can distinguish between unknown transport mechanisms that describe the interfacial phenomena. Furthermore, sensitivity analysis (e.g., contours), as demonstrated above, help visualize the inherent trade-off that exists within model parameters and determine whether the data supports the inclusion of additional transport and thermodynamic phenomena.

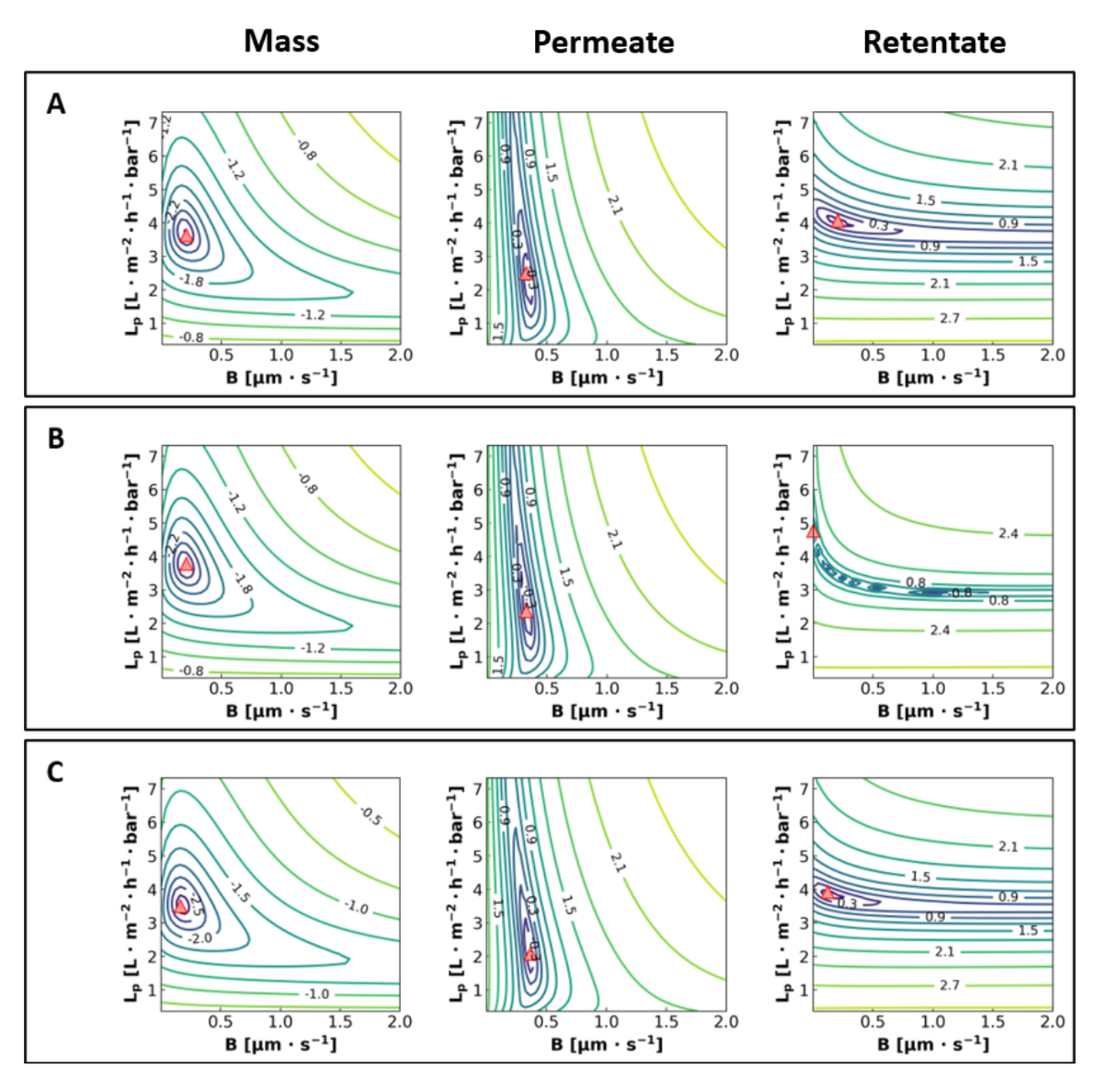


Fig. 6: Residual squared contours comparing the hydraulic permeability and solute permeability coefficient for **diafil-tration** experiments. Two different models (with concentration polarization & without concentration polarization) and two data set variations (data with an inline conductivity sensor & data encompassing only the initial and final in-situ retentate measurements) are evaluated. The model used to generate the contours of panel A includes concentration polarization with the inline conductivity probe measurements. The residual squared contours of panel B were calculated using a reduced data set which excludes the semi-continuous retentate data. Panel C contours evaluate model in which the inline conductivity measurements were used yet concentration polarization is not accounted for.

5. Conclusions

Within this study, we demonstrate that a diafiltration apparatus, designed to modulate the stirred cell concentration over the course of an experiment, can overcome many of the limitations that are inherent to filtration experiments. The incorporation of an inline conductivity probe provides key information on the path taken by the retentate concentration, in turn identifying a unique reflection coefficient and differentiating between rejection-based and adsorption-based removal processes. Moreover, the coupling of data analytics and instrumentation led to the identification of governing membrane parameters five times more quickly than traditional techniques. The framework presented within this study will help differentiate the transport mechanisms that govern membrane separations, ultimately providing fundamental insight on how molecular level changes impact macroscopic system properties. The current framework uses transport coefficients that are not concentration dependent. However, future extensions of the apparatus will seek to study transport through membranes that exhibit explicit concentration dependent properties. As the device detailed in this effort is extended to study other membrane systems, two situations may arise. First, several candidate models capable of detailing transport and interfacial phenomena through a particular membrane may exist but there is ambiguity regarding which model best describes the system. In this instance, a set of experiments can be designed by applying model discrimination criteria from MBDoE. By being able to discriminate between the series of candidate models, researchers can gain insights into which molecular characteristics should be modified to enhance membrane performance. Alternatively, models that capture the concentration-dependent behavior of a system may not exist. In this case, the framework would need to be modified. For example, transport parameters could be regressed for the individual permeate vials. These vial-specific parameters can be presented as a function of the average solute concentration within the stirred cell, which is measured during sample collection using the inline conductivity probe. This analysis provides concentration dependent parameters that can be fit to complex relationships and related to specific membrane properties (e.g., surface charge). When functionalized with specific ligands (e.g., diamines), membranes have been shown to exhibit concentration dependent transport properties [55, 56]. Future developments will focus on studying ligand solute interactions within molecularly engineered membranes, thereby elucidating the relationship between the solute-membrane interaction strength and corresponding transport mechanism.

Notation

	$\Delta\pi$	osmotic pressure	bar
500	ΔP	applied pressure	bar
	ν	kinematic viscosity of the solvent	${\rm cm}^2\cdot {\rm s}^{-1}$
	ρ	density of the solution	$\mathrm{g}\cdot\mathrm{cm}^{-3}$
	ρ	density of the solution	$\mathrm{g}\cdot\mathrm{cm}^{-3}$
	σ	thermodynamic reflection coefficient	dimensionless
505	A_m	area of the membrane	${ m cm}^2$
	A_m	area of the membrane	${\rm cm}^2$
	B	solute permeability coefficient	${\rm cm\cdot s^{-1}}$
	b	diameter of the stirred cell	cm
	c_d	concentration in the feed solution	$\mu \text{mol} \cdot \text{cm}^{-3}, \text{mM}$
510	c_d	concentration in the feed solution	$\mu \text{mol} \cdot \text{cm}^{-3}, \text{ mM}$
	c_f	dynamic concentration in the feed solution	$\mu \text{mol} \cdot \text{cm}^{-3}, \text{ mM}$
	c_h	dynamic concentration within hold-up volume	$\mu \text{mol} \cdot \text{cm}^{-3}, \text{ mM}$
	c_v	dynamic concentration in the sample vial	$\mu \text{mol} \cdot \text{cm}^{-3}, \text{ mM}$
	c_v	dynamic concentration in the sample vial	$\mu \text{mol} \cdot \text{cm}^{-3}, \text{ mM}$
515	c_{in}	dynamic concentration at the feed-side solution-membrane interface	
			$\mu \text{mol} \cdot \text{cm}^{-3}, \text{ mM}$
	D	diffusion coefficient of the solute in the solvent	${\rm cm}^2\cdot {\rm s}^{-1}$
	J_s	solute flux across the membrane	$\mu \mathrm{mol} \cdot \mathrm{cm}^{-2} \cdot \mathrm{s}^{-1}$
	J_w	water flux across the membrane	${\rm cm\cdot s^{-1}}$

520	k	mass transfer coefficient of interest	${\rm cm}\cdot{\rm s}^{-1}$
	L_p	hydraulic permeability coefficient	$\rm cm\cdot bar^{-1}\cdot s^{-1}$
	m_d	mass of the diafiltrate reservoir	g
	m_d	mass of the diafiltrate reservoir	g
	m_f	mass of the filtration cell	g
525	m_f	mass of the filtration cell	g
	m_h	mass of solution in holdup	g
	m_h	mass of solution in holdup	g
	m_v	mass of the sample vial	g
	m_v	mass of the sample vial	g
530	N	number of measurements for a vial	dimensionless
	n	number of dissolved species	dimensionless
	R	gas constant	cm³· bar · μ mol ⁻¹ · K ⁻¹
	s	precision for different measurements	g or mM
	T	temperature	K
535	v^0	average velocity within the stirred cell	${ m cm}\cdot{ m s}^{-1}$
	w	weight for residual squared	g^{-2} or mM^{-2}

Acknowledgments

This work was made possible with support from the National Science Foundation (NSF) through the Advanced Manufacturing Program (Award Number: 1932206), and we appreciatively acknowledge this support. This work was partially supported by the Bureau of Reclamation, Department of Interior, via DWPR Agreement R18AC00116 and by the NSF through the CAREER Program (Award Number: CBET-1941596). We would like to thank the Center for Environmental Science

and Technology at the University of Notre Dame (CEST) portions of this research was performed with instruments at this facility. D.J.B. gratefully acknowledges support for this project from the Vincent P. Slatt Fellowship for Undergraduate Research in Energy Systems and Processes, administered by the Center for Sustainable Energy at Notre Dame. E.A.E. gratefully acknowledges support from the Patrick and Jana Eilers Graduate Student Fellowship for Energy Related Research at the University of Notre Dame.

Conflict of interest statement

Nothing to declare.

References

555

560

- [1] M. Elimelech, W. A. Phillip, The future of seawater desalination: energy, technology, and the environment, Science 333 (6043) (2011) 712–717.
- [2] A. L. Zydney, New developments in membranes for bioprocessing—a review, Journal of Membrane Science (2020) 118804.
 - [3] I. Manzano, N. Taylor, M. Csordas, G. E. Vezeau, H. M. Salis, A. L. Zydney, Purification of Cas9—RNA complexes by ultrafiltration, Biotechnology Progress 37 (2) (2021) e3104.
 - [4] T. Corrado, R. Guo, Macromolecular design strategies toward tailoring free volume in glassy polymers for high performance gas separation membranes, Molecular Systems Design & Engineering 5 (1) (2020) 22–48.
 - [5] T. Corrado, Z. Huang, J. Aboki, R. Guo, Microporous polysulfones with enhanced separation performance via integration of the triptycene moiety, Industrial & Engineering Chemistry Research 59 (12) (2019) 5351–5361.
- [6] J. R. Werber, A. Deshmukh, M. Elimelech, The critical need for increased selectivity, not increased water permeability, for desalination membranes, Environmental Science & Technology Letters 3 (4) (2016) 112–120.
- [7] J. R. Hoffman, W. A. Phillip, 100th anniversary of macromolecular science viewpoint: Integrated membrane systems, ACS Macro Letters 9 (9) (2020) 1267–1279.

[8] R. Sujanani, M. R. Landsman, S. Jiao, J. D. Moon, M. S. Shell, D. F. Lawler, L. E. Katz, B. D. Freeman, Designing solute-tailored selectivity in membranes: Perspectives for water reuse and resource recovery, ACS Macro Letters 9 (11) (2020) 1709–1717.

570

575

- [9] National Academies of Sciences, Engineering, and Medicine, A Research Agenda for Transforming Separation Science, National Academies Press, 2019.
- [10] R. Z. Waldman, F. Gao, W. A. Phillip, S. B. Darling, Maximizing selectivity: An analysis of isoporous membranes, Journal of Membrane Science (2021) 119389.
- [11] X. Qiu, H. Yu, M. Karunakaran, N. Pradeep, S. P. Nunes, K.-V. Peinemann, Selective separation of similarly sized proteins with tunable nanoporous block copolymer membranes, ACS Nano 7 (1) (2013) 768–776.
- [12] C. Osuji, P. J. Ferreira, G. Mao, C. K. Ober, J. B. Vander Sande, E. L. Thomas, Alignment of self-assembled hierarchical microstructure in liquid crystalline diblock copolymers using high magnetic fields, Macromolecules 37 (26) (2004) 9903–9908.
 - [13] E. S. Hatakeyama, C. J. Gabriel, B. R. Wiesenauer, J. L. Lohr, M. Zhou, R. D. Noble, D. L. Gin, Water filtration performance of a lyotropic liquid crystal polymer membrane with uniform, sub-1-nm pores, Journal of Membrane Science 366 (1-2) (2011) 62–72.
- [14] A. Zirehpour, A. Rahimpour, M. Ulbricht, Nano-sized metal organic framework to improve the structural properties and desalination performance of thin film composite forward osmosis membrane, Journal of Membrane Science 531 (2017) 59–67.
 - [15] J. L. Fenton, D. W. Burke, D. Qian, M. Olvera de la Cruz, W. R. Dichtel, Polycrystalline covalent organic framework films act as adsorbents, not membranes, Journal of the American Chemical Society 143 (3) (2021) 1466–1473.
 - [16] D. Zhu, X. Li, Y. Li, M. Barnes, C.-P. Tseng, S. Khalil, M. M. Rahman, P. M. Ajayan, R. Verduzco, Transformation of one-dimensional linear polymers into two-dimensional covalent organic frameworks through sequential reversible and irreversible chemistries, Chemistry of Materials (2020).

- [17] F. Gao, A. Hunter, S. Qu, J. R. Hoffman, P. Gao, W. A. Phillip, Interfacial junctions control electrolyte transport through charge-patterned membranes, ACS Nano 13 (7) (2019) 7655– 7664.
 - [18] I. Sadeghi, A. Asatekin, Membranes with functionalized nanopores for aromaticity-based separation of small molecules, ACS Applied Materials & Interfaces 11 (13) (2019) 12854–12862.
- [19] S. Benavides, S. Qu, F. Gao, W. A. Phillip, Polymeric ion pumps: Using an oscillating stimulus to drive solute transport in reactive membranes, Langmuir 34 (15) (2018) 4503–4514.
 - [20] J. Lu, H. Zhang, J. Hou, X. Li, X. Hu, Y. Hu, C. D. Easton, Q. Li, C. Sun, A. W. Thornton, et al., Efficient metal ion sieving in rectifying subnanochannels enabled by metal-organic frameworks, Nature materials (2020) 1–8.
- [21] H. Zhang, X. Hou, L. Zeng, F. Yang, L. Li, D. Yan, Y. Tian, L. Jiang, Bioinspired artificial single ion pump, Journal of the American Chemical Society 135 (43) (2013) 16102–16110.
 - [22] Y. Zhang, G. C. Schatz, Advantages of conical pores for ion pumps, The Journal of Physical Chemistry C 121 (1) (2017) 161–168.
 - [23] E. Cussler, Membranes which pump, AIChE Journal 17 (6) (1971) 1300–1303.
- [24] E. L. Cussler, Multicomponent diffusion, Vol. 3, Elsevier, 2013.
 - [25] J. Lamb, J. Christensen, S. Izatt, K. Bedke, M. Astin, R. Izatt, Effects of salt concentration and anion on the rate of carrier-facilitated transport of metal cations through bulk liquid membranes containing crown ethers, Journal of the American Chemical Society 102 (10) (1980) 3399–3403.
- [26] V. S. Rathee, S. Qu, W. A. Phillip, J. K. Whitmer, A coarse-grained thermodynamic model for the predictive engineering of valence-selective membranes, Molecular Systems Design & Engineering 1 (3) (2016) 301–312.
- [27] X. Zhou, Z. Wang, R. Epsztein, C. Zhan, W. Li, J. D. Fortner, T. A. Pham, J.-H. Kim,
 M. Elimelech, Intrapore energy barriers govern ion transport and selectivity of desalination
 membranes, Science Advances 6 (48) (2020) eabd9045.

- [28] C. Cheng, A. Yaroshchuk, M. L. Bruening, Fundamentals of selective ion transport through multilayer polyelectrolyte membranes, Langmuir 29 (6) (2013) 1885–1892.
- [29] Z. Zhang, M. M. Rahman, C. Abetz, A.-L. Höhme, E. Sperling, V. Abetz, Chemically tailored multifunctional asymmetric isoporous triblock terpolymer membranes for selective transport, Advanced Materials 32 (8) (2020) 1907014.

- [30] J. Shao, A. L. Zydney, Optimization of ultrafiltration/diafiltration processes for partially bound impurities, Biotechnology and Bioengineering 87 (3) (2004) 286–292.
- [31] R. Ghosh, Z. Cui, Analysis of protein transport and polarization through membranes using pulsed sample injection technique, Journal of Membrane Science 175 (1) (2000) 75–84.
- [32] R. Ghosh, Y. Wan, Z. Cui, G. Hale, Parameter scanning ultrafiltration: rapid optimisation of protein separation, Biotechnology and bioengineering 81 (6) (2003) 673–682.
 - [33] E. A. Eugene, W. A. Phillip, A. W. Dowling, Data science-enabled molecular-to-systems engineering for sustainable water treatment, Current Opinion in Chemical Engineering 26 (2019) 122–130.
- [34] J. Liu, B. McCool, J. Johnson, N. Rangnekar, P. Daoutidis, M. Tsapatsis, Mathematical modeling and parameter estimation of mfi membranes for para/ortho-xylene separation, AIChE Journal (2021) e17232.
 - [35] A. Altaee, Computational model for estimating reverse osmosis system design and performance: Part-one binary feed solution, Desalination 291 (2012) 101–105.
- [36] J. Garcia-Aleman, J. M. Dickson, Mathematical modeling of nanofiltration membranes with mixed electrolyte solutions, Journal of Membrane Science 235 (1-2) (2004) 1–13.
 - [37] G. Franceschini, S. Macchietto, Model-based design of experiments for parameter precision: State of the art, Chemical Engineering Science 63 (19) (2008) 4846–4872.
- [38] W. J. Hill, W. G. Hunter, D. W. Wichern, A joint design criterion for the dual problem of model discrimination and parameter estimation, Technometrics 10 (1) (1968) 145–160.

- [39] G. B. Ferraris, P. Forzatti, G. Emig, H. Hofmann, Sequential experimental design for model discrimination in the case of multiple responses, Chemical Engineering Science 39 (1) (1984) 81–85.
- [40] M. Schwaab, F. M. Silva, C. A. Queipo, A. G. Barreto Jr, M. Nele, J. C. Pinto, A new approach for sequential experimental design for model discrimination, Chemical Engineering Science 61 (17) (2006) 5791–5806.
 - [41] F. Galvanin, R. Marchesini, M. Barolo, F. Bezzo, M. Fidaleo, Optimal design of experiments for parameter identification in electrodialysis models, Chemical Engineering Research and Design 105 (2016) 107–119. doi:10.1016/j.cherd.2015.10.048.
- [42] F. Galvanin, E. Cao, N. Al-Rifai, A. Gavriilidis, V. Dua, A joint model-based experimental design approach for the identification of kinetic models in continuous flow laboratory reactors, Computers & Chemical Engineering 95 (2016) 202–215.
 - [43] L. T. Biegler, Nonlinear programming: concepts, algorithms, and applications to chemical processes, SIAM, 2010.
- [44] K. D. Dorfman, P. Daoutidis, Numerical Methods with Chemical Engineering Applications, Cambridge University Press, 2017.
 - [45] O. Kedem, A. Katchalsky, Thermodynamic analysis of the permeability of biological membranes to non-electrolytes, Biochimica et Biophysica Acta 27 (1958) 229–246.
- [46] S. Yang, N. Wang, A novel p systems based optimization algorithm for parameter estimation of
 proton exchange membrane fuel cell model, International Journal of Hydrogen Energy 37 (10)
 (2012) 8465–8476.
 - [47] S. Sundaramoorthy, G. Srinivasan, D. Murthy, An analytical model for spiral wound reverse osmosis membrane modules: Part i—model development and parameter estimation, Desalination 280 (1-3) (2011) 403–411.
- [48] Zeman, A. L. Zydney, Microfiltration and ultrafiltration: principles and applications, CRC Press, 1996.

- [49] H. Al-Zoubi, N. Hilal, N. Darwish, A. Mohammad, Rejection and modelling of sulphate and potassium salts by nanofiltration membranes: neural network and spiegler–kedem model, Desalination 206 (1-3) (2007) 42–60.
- [50] A. Pankajakshan, C. Waldron, M. Quaglio, A. Gavriilidis, F. Galvanin, A multi-objective optimal experimental design framework for enhancing the efficiency of online model identification platforms, Engineering 5 (6) (2019) 1049–1059.
 - [51] C. Waldron, A. Pankajakshan, M. Quaglio, E. Cao, F. Galvanin, A. Gavriilidis, Closed-loop model-based design of experiments for kinetic model discrimination and parameter estimation: Benzoic acid esterification on a heterogeneous catalyst, Industrial & Engineering Chemistry Research 58 (49) (2019) 22165–22177.

680

- [52] M. Quaglio, C. Waldron, A. Pankajakshan, E. Cao, A. Gavriilidis, E. S. Fraga, F. Galvanin, An online reparametrisation approach for robust parameter estimation in automated model identification platforms, Computers & Chemical Engineering 124 (2019) 270–284.
- [53] D. Vlachos, A. Mhadeshwar, N. S. Kaisare, Hierarchical multiscale model-based design of experiments, catalysts, and reactors for fuel processing, Computers & Chemical Engineering 30 (10-12) (2006) 1712–1724.
 - [54] C. Tsay, R. C. Pattison, M. Baldea, B. Weinstein, S. J. Hodson, R. D. Johnson, A superstructure-based design of experiments framework for simultaneous domain-restricted model identification and parameter estimation, Computers & Chemical Engineering 107 (2017) 408–426.
 - [55] S. Qu, T. Dilenschneider, W. A. Phillip, Preparation of chemically-tailored copolymer membranes with tunable ion transport properties, ACS applied materials & interfaces 7 (35) (2015) 19746–19754.
- [56] F. Fornasiero, H. G. Park, J. K. Holt, M. Stadermann, C. P. Grigoropoulos, A. Noy, O. Bakajin, Ion exclusion by sub-2-nm carbon nanotube pores, Proceedings of the National Academy of Sciences 105 (45) (2008) 17250–17255.

Supplementary Information for

DATA: Diafiltration Apparatus for high-Throughput Analysis

Jonathan A. Ouimet, Xinhong Liu, David J. Brown, Elvis A. Eugene, Tylar Popps, Zachary W. Muetzel, Alexander W. Dowling, William A. Phillip¹

Department of Chemical and Biomolecular Engineering, University of Notre Dame, Notre Dame, IN 46556

February 2, 2022

S1. Model Derivation

Note that Fig. 1, Eq. (1), etc. refer to elements of the main text. Fig. S1, Eq. (S1), etc. are unique to the supplementary information.

In order to infer the three governing parameters in Eqs. (1) and (2), we conduct mass and solute balances around three control volumes within Fig. 1, the diafiltrate reservoir, the stirred cell, and the permeate. By assuming Fig. 1 represents a closed system, where the solution density is invariant to the salt concentration, the mass exiting the diafiltrate reservoir must be equal to the mass of water permeating through the membrane, Eq. (S1).

$$\frac{dm_d}{dt} = -A_m \rho J_w \tag{S1}$$

where m_d is the mass of the diafiltrate reservoir, A_m is the membrane area and ρ is the density of the solution. As the diafiltrate concentration is defined before the experiment begins and nothing enters the diafiltrate reservoir, the diafiltrate concentration remains constant during each experiment, Eq. (S2).

$$\frac{dc_d}{dt} = 0 (S2)$$

Within our second control volume, the stirred cell, we enforce a constant volume system, i.e., Eq. (S3), by experimentally ensuring the volumetric flow rate of diafiltrate into the stirred cell is equal to the flow rate of the permeate across the membrane.

$$\frac{dm_f}{dt} = 0 \tag{S3}$$

The solute within the stirred cell is modeled by finding the difference between the solute entering (i.e., from the diafiltrate) and the solute transported across the membrane, Eq. (S4). The left hand side of Eq. (S4) can be simplified by applying the product rule and substituting in Eq. (S3). This provides Eq. (5) which describes the changing concentration within the stirred cell.

$$\frac{d(c_f m_f)}{dt} = A_m \rho (J_w c_d - J_s) \tag{S4}$$

¹corresponding author: wphillip@nd.edu

$$\frac{d(c_f m_f)}{dt} = m_f \frac{dc_f}{dt} + c_f \frac{dm_f}{dt} \tag{S5}$$

$$\frac{dc_f}{dt} = \frac{A_m \rho}{m_f} (J_w c_d - J_s) \tag{5}$$

The final control volume encompasses the hold up volume, the transfer tube, and the scintillation vial. Equation (S6) states the permeate mass in this control volume remains constant during each experiment.

$$\frac{dm_h}{dt} = 0 \tag{S6}$$

The amount of solute in the hold-up volume is provided by the difference of the solute transported through the membrane and the solute collected within the scintillation vial, Eq. (S7). Substituting Eq. (7) into Eq. (S7) yields Eq. (6).

$$\frac{d(c_h m_h)}{dt} = A_m \rho J_s - \frac{dm_v}{dt} c_h \tag{S7}$$

$$\frac{dm_v}{dt} = -\frac{dm_d}{dt} = A_m \rho J_w \tag{7}$$

$$\frac{dc_h}{dt} = \frac{A_m \rho}{m_h} (J_s - c_h J_w) \tag{6}$$

The time dependent concentration of the scintillation vial is expressed by Eq. (8). As described previously, the product rule, Eq. (S8) is used to derive Eq. (S9) which captures the changing vial concentration.

$$\frac{d(c_v m_v)}{dt} = \frac{dm_v}{dt} c_h = A_m \rho J_w c_h \tag{8}$$

$$\frac{d(c_v m_v)}{dt} = m_v \frac{dc_v}{dt} + c_v \frac{dm_v}{dt} \tag{S8}$$

$$\frac{dc_v}{dt} = \frac{dm_d}{dt} \frac{(c_v - c_h)}{m_v} = -A_m \rho J_w \frac{(c_v - c_h)}{m_v}$$
(S9)

S2. Supplementary Figures

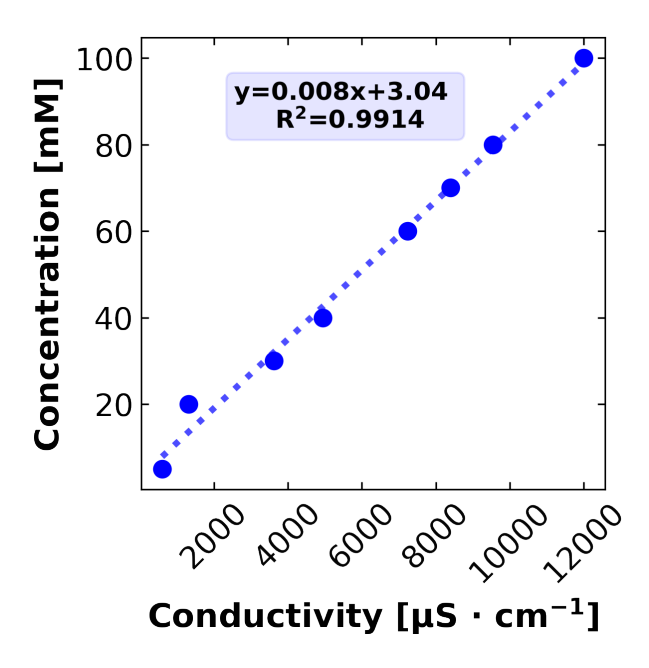


Fig. S1: The calibration curve used to convert conductivity measurements into the corresponding KCl concentration. The conductivity was calculated using, $C = GAV^{-1}$, the relationship between the conductivity probe cell constant (G = 0.42 cm⁻¹), the peak to peak applied current, (A = 1 mA), and the peak to peak differential voltage drop, V.

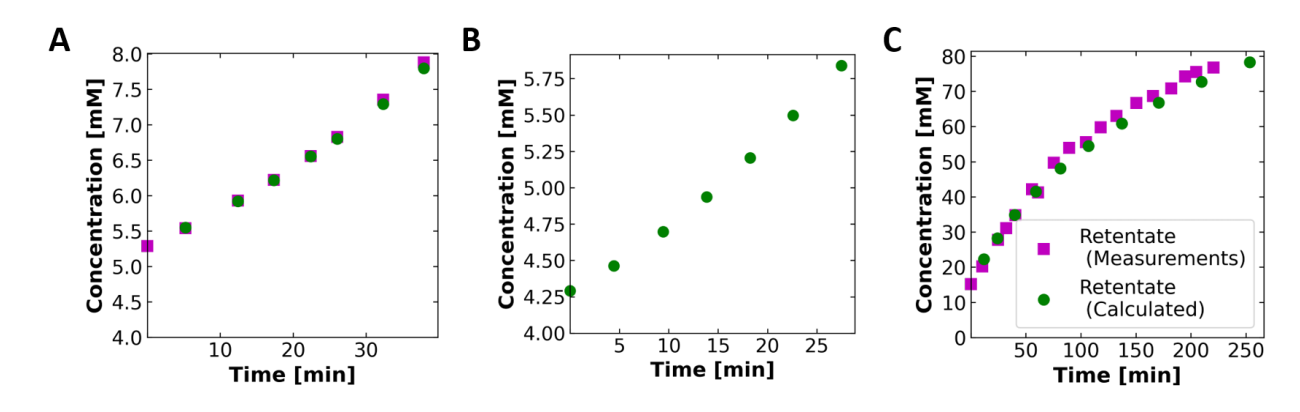


Fig. S2: Panel A presents a filtration experiment run at 40% recovery. The lower recovery allows the semi-continuous monitoring of the retentate with the inline conductivity probe (purple squares). Mass balance calculations (green circles) corroborate the conductivity measurements. Panel B presents the retentate concentration data, predicted by mass calculations (green circles), of a filtration experiment run at 60% recovery. The inline conductivity probe was not used as the high percent recovery decreased the volume of solution in the stirred cell below the sensor. Panel C presents information for a diafiltration experiment. The retentate concentration (purple squares) measured by the inline conductivity probe agrees with the the retentate concentration predicted from mass balance calculations (green circles). For filtration experiments, the calculated retentate concentration values were obtained by subtracting the total moles of solute in the permeate from the initial feed value and adjusting the stirred cell volume to account for the mass of solution in the permeate. Within diafiltration experiments, the stirred cell volume was kept constant. The change in solute within the stirred cell is calculated as the difference from the entering diafiltrate solute and exiting permeate solute. To calculate the new retentate concentration, the adjusted stirred cell solute amount is divided by the total volume.

Table S1: The time required to characterize a membrane over the phase space of interest (i.e., 5 mM - 80 mM) for filtration and diafiltration experiments are compared. Approximately 5 mL of DI water were run through the membranes before each experiment. Filtration experiments were run at 30% - 40% recovery with the inline conductivity probe; a total of 9 samples were collected from each experiment. Within the diafiltration experiments, an 80 mM diafiltrate concentration was used and a total of 13 samples were collected. The ICP-OES preparation and run time calculations were determined from the number of samples collected within the experiment. The analysis conducted consists of mass balances to ensure that all the solute entering the stirred cell was accounted for within the final retentate and permeate samples. While one diafiltration experiment covers the entire concentration range of interest, it would require approximately 10 filtration experiments to obtain an equal amount of information.

Filtration and Diafiltration Time Comparison						
		Filtration	Diafiltration			
Avg. Samples Collected:	-	9	13			
Avg. Permeated Mass:	gram	3.8	10.8			
Experimental Set-up Time:	minute	20	20			
Avg. Experiment Run Time:	minute	40	213			
Membrane Rinse/Wash:	minute	60	60			
Data Analysis (ICP) Prep. Time:	minute	36	52			
ICP Run Time:	minute	67	79			
Long Hand Analysis/Balances:	minute	60	60			
Experimental Time:	minute	283	484			
Phase Space Consideration:	experiment	10	1			
Total Time:	minute	2830	484			

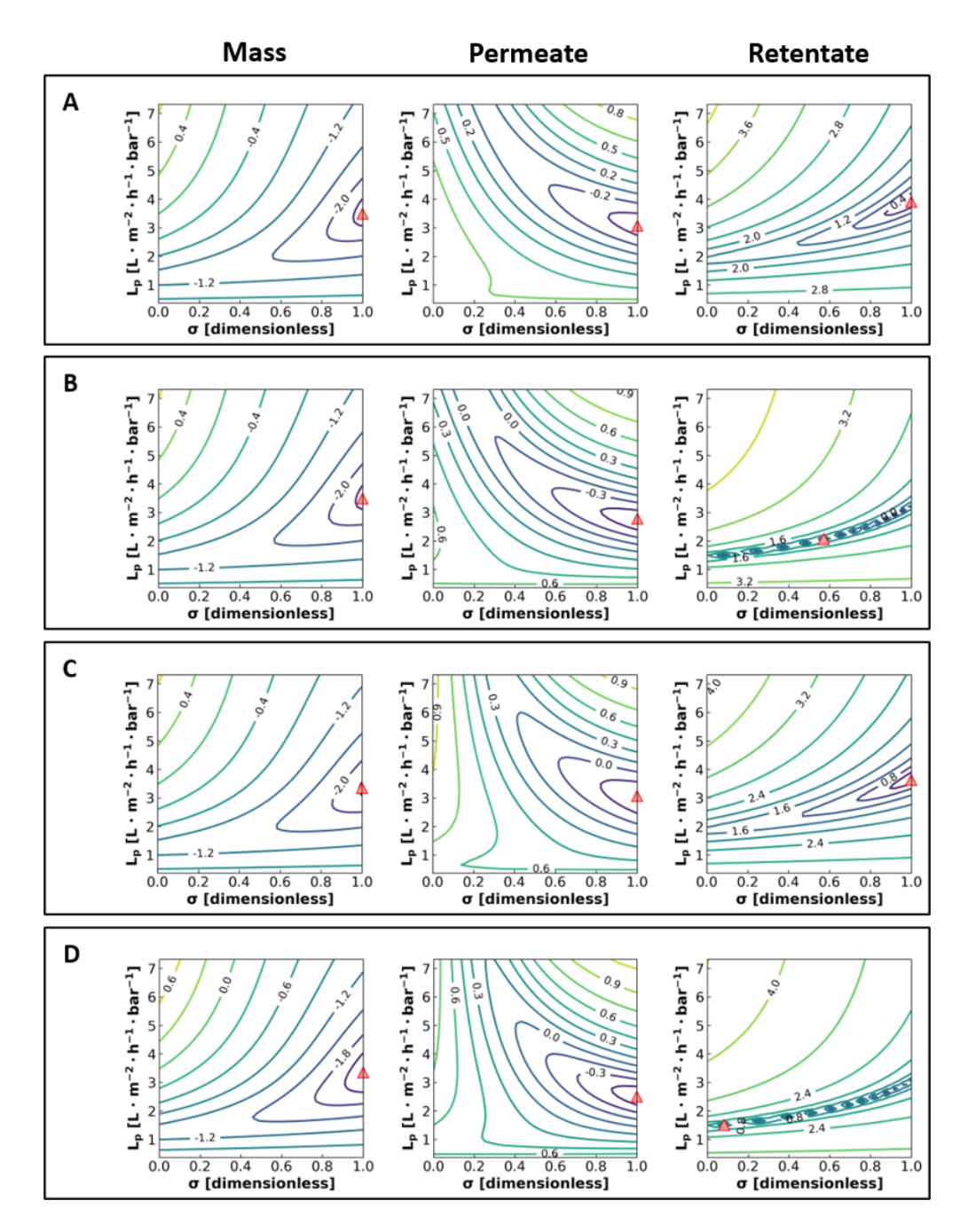


Fig. S3: Residual squared contours comparing the reflection coefficient and hydraulic permeability for **diafiltration** experiments. Two different models (with concentration polarization & without concentration polarization) and two data set variations (data with an inline conductivity sensor & data encompassing only the initial and final in-situ retentate measurements) are evaluated. The model used to generate the contours of panel A includes concentration polarization phenomena with the inline conductivity probe measurements. The residual squared contours of panel B uses a reduced data set which excludes the semi-continuous retentate data. Panel C contours evaluate a separate model in which the inline conductivity measurements are used yet concentration polarization is not accounted for. The contours generated in panel D use the reduced data set and neglect concentration polarization.

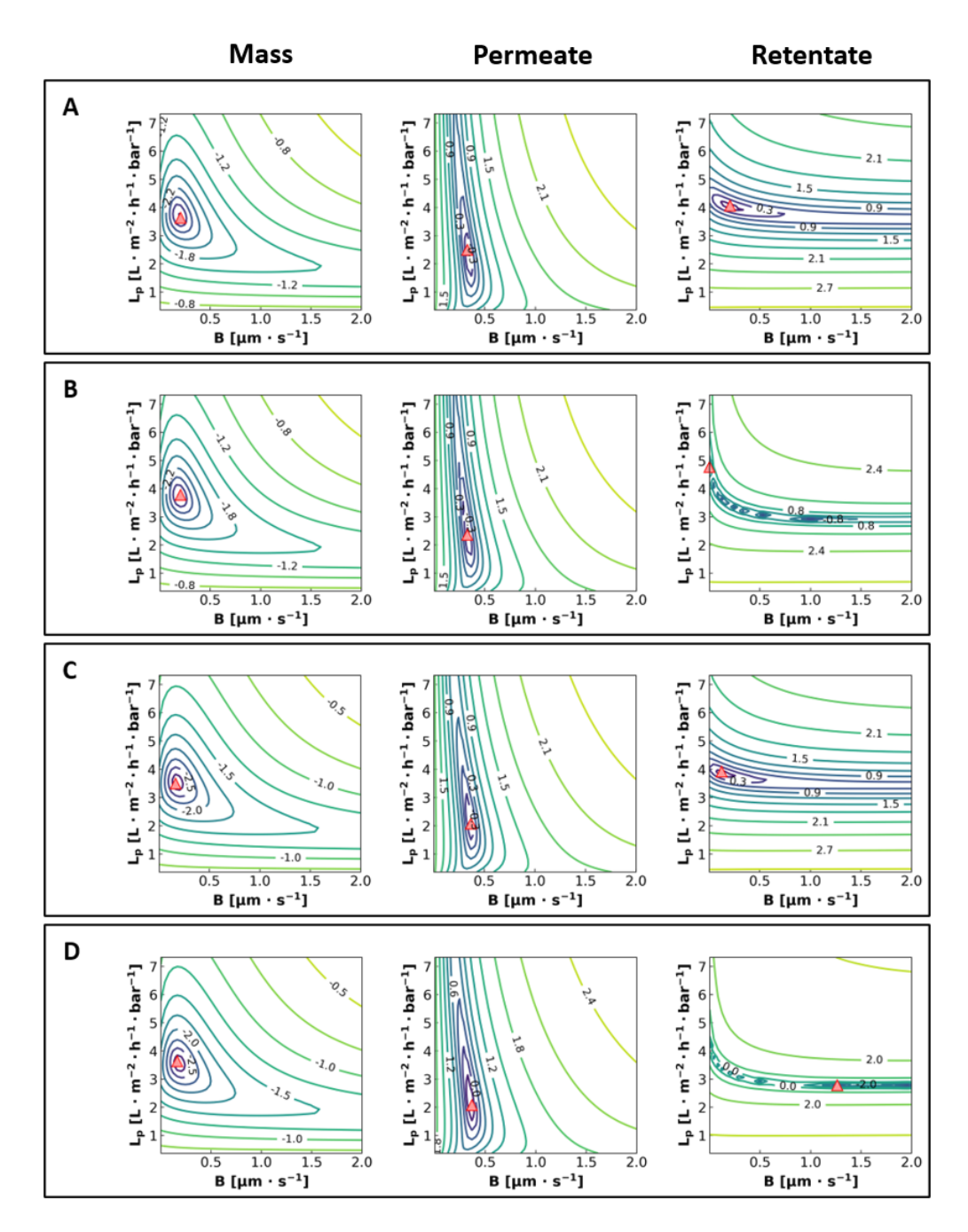


Fig. S4: Residual squared contours comparing the hydraulic permeability and solute permeability coefficient for **diafiltration** experiments. Two different models (with concentration polarization & without concentration polarization) and two data set variations (data with an inline conductivity sensor & data encompassing only the initial and final in-situ retentate measurements) are evaluated. The model used to generate the contours of panel A includes concentration polarization phenomena with the inline conductivity probe measurements. The residual squared contours of panel B uses a reduced data set which excludes the semi-continuous retentate data. Panel C contours evaluate a separate model in which the inline conductivity measurements are used yet concentration polarization is not accounted for. The contours generated in panel D use the reduced data set and do not incorporate concentration polarization.

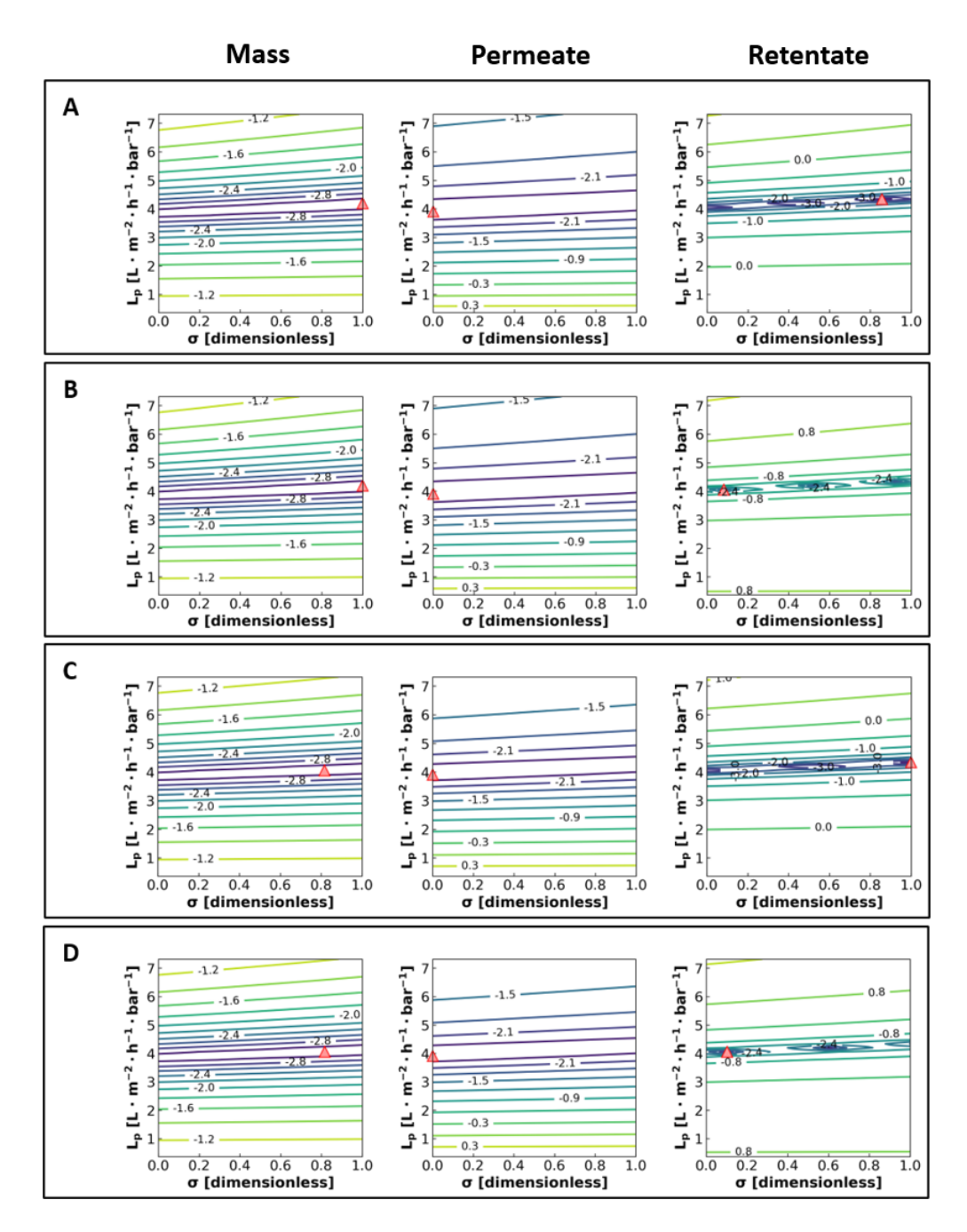


Fig. S5: Residual squared contours comparing the hydraulic permeability and reflection coefficient for of filtration experiments. Two different models (with concentration polarization & without concentration polarization) and two data set variations (data with an inline conductivity sensor & data encompassing only the initial and final in-situ retentate measurements) are evaluated. The model used to generate the contours of panel A includes concentration polarization phenomena with the inline conductivity probe measurements. The residual squared contours of panel B uses a reduced data set which excludes the semi-continuous retentate data. Panel C contours evaluate a separate model in which the inline conductivity measurements are used yet concentration polarization is not accounted for. The contours generated in panel D use the reduced data set and ignore concentration polarization.

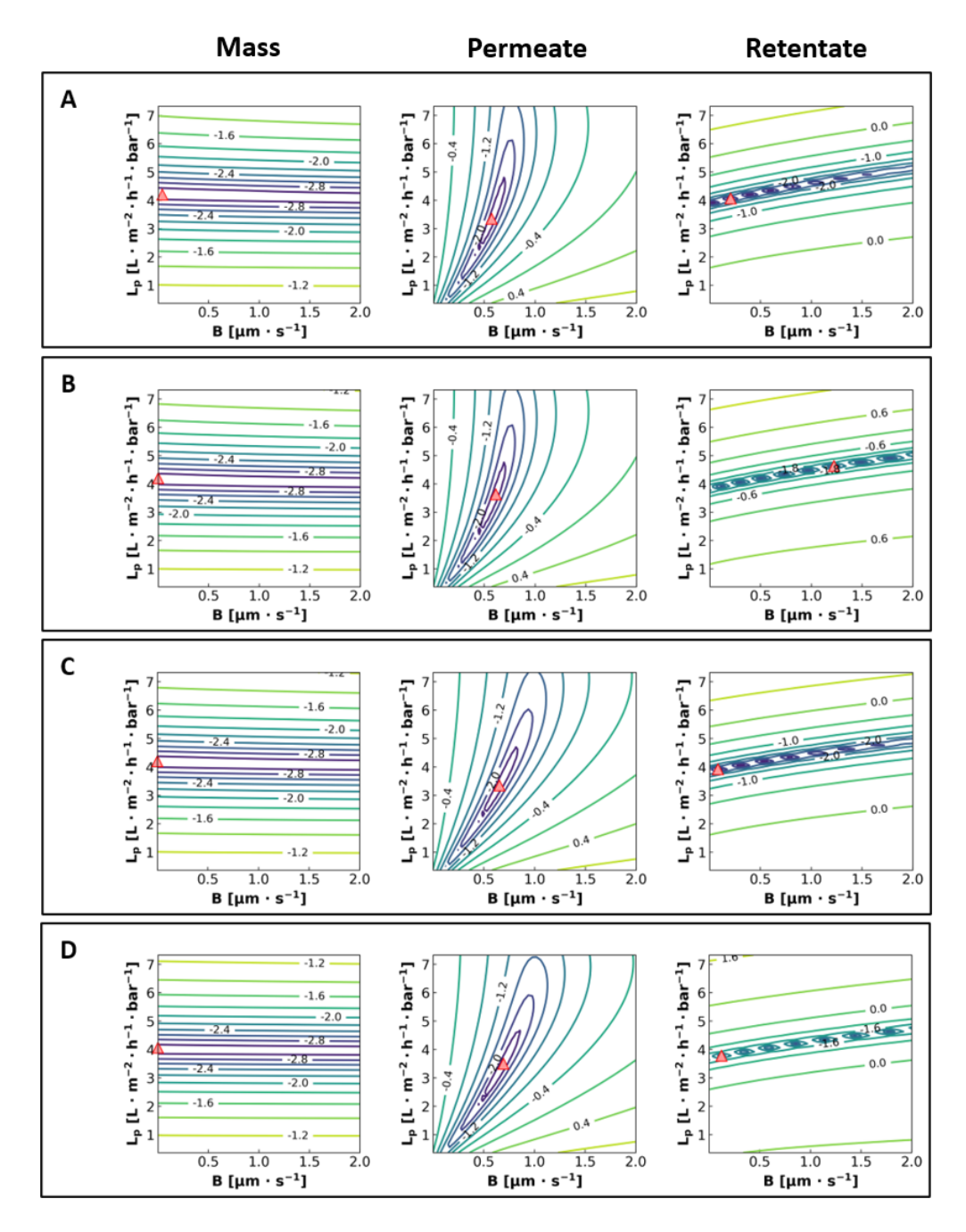


Fig. S6: Residual squared contours comparing the hydraulic permeability and solute permeability coefficient for of filtration experiments. Two different models (with concentration polarization & without concentration polarization) and two data set variations (data with an inline conductivity sensor & data encompassing only the initial and final in-situ retentate measurements) are evaluated. The model used to generate the contours of panel A includes concentration polarization phenomena with the inline conductivity probe measurements. The residual squared contours of panel B uses a reduced data set which excludes the semi-continuous retentate data. Panel C contours evaluate a separate model in which the inline conductivity measurements are used yet concentration polarization is not accounted for. The contours generated in panel D use the reduced data set and neglect concentration polarization.

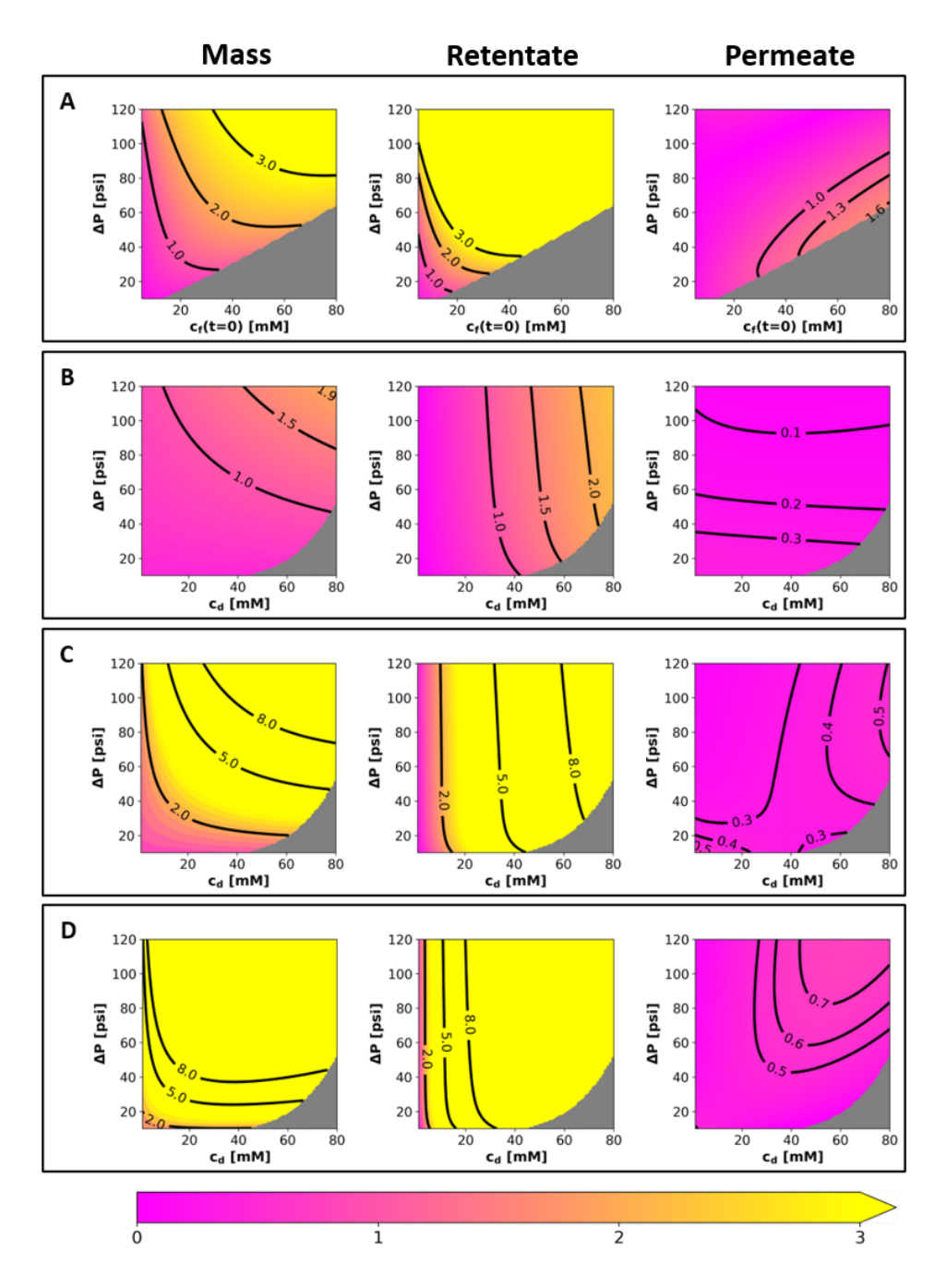


Fig. S7: Filtration and diafiltration experiments were modeled under varying initial feed or diafiltrate concentrations and applied pressures to determine the conditions necessary to differentiate reflection coefficients with a precision equal to 0.1. Panel A models a filtration experiment where the initial feed concentration and applied pressure are varied. Panels B, C, and D vary the applied pressure and diafiltrate concentration of a diafiltration experiment run with an initial feed concentration of 5mM. Panels B, C, and D correspond to the data gathered after the 1^{st} , 5^{th} , and 10^{th} vials, respectively. The contours are generated using the L_p , B, σ values from Membrane A & M1 presented in Table 2. The contours represent the difference in model predictions via equations (7),(5), and (S9) from two different sigma values (i.e., $\sigma = 0.9$ and $\sigma = 1$) normalized by the precision of the measuring instruments. Thus the contour lines are dimensionless. The shaded area in the bottom right of the graphs correspond to non-physical systems in which the flux is equal to or less than zero (i.e., the osmotic pressure is equal to or greater than the applied pressure.)